Quaternary Science Reviews 286 (2022) 107529

Contents lists available at ScienceDirect

Quaternary Science Reviews

journal homepage: www.elsevier.com/locate/quascirev

The multifaceted history of the Walker Circulation during the Plio-Pleistocene

Stefanie Kaboth-Bahr [a, *], Manfred Mudelsee [a, b, c, d]

[a] University of Potsdam, Institute of Geosciences, Potsdam, Germany
[b] Climate Risk Analysis, Bad Gandersheim, Germany
[c] Advanced Climate Risk Education, Bad Gandersheim, Germany
[d] Alfred Wegener Institute Helmholtz Centre for Polar and Marine Research, Bremerhaven, Germany

ARTICLE INFO

Article history:
Received 31 July 2021
Received in revised form
20 April 2022
Accepted 20 April 2022
Available online xxx

Handling Editor: Dr A. Voelker

Keywords:
Walker circulation
Plio-pleistocene transition
Early pleistocene
Statistical analysis
Change-point regression model

ABSTRACT

The Walker Circulation (WC) is an east-west trending band of atmospheric circulation cells along the equator and the predominant controller of heat and moisture transport in the tropics. Its variability is closely linked to the sea-surface temperature (SST) changes across the Pacific, the Indian and the Atlantic Oceans and can have pronounced effects on the humidity regimes of the adjacent continents. In recent years, the evolution of the WC during the Plio- and Pleistocene epochs has been intensely studied in the context of the effectiveness of the tropics in modulating global climate change (e.g., the intensification of Northern Hemisphere glaciation).

However, the onset of the modern WC pattern as well as its global impact during the Plio- and Pleistocene is controversially assessed in the literature. For its onset, previous studies have suggested dates ranging between 2.4 and 0.8 million years ago (Myr), while its argued impact ranges from – crucially influencing the increase of Northern Hemisphere ice sheet growth by channelling heat and moisture from the tropics into the high latitudes to – having no effect on global ice volume changes. In order to achieve a comprehensive understanding of the spatiotemporal evolution of the WC during this time frame, we statistically analysed 30 globally distributed SST records covering the low and high latitudes between 3.5 and 1.5 Myr, encompassing the Late Pliocene to Early Pleistocene. We utilized a statistical change-point regression model to determine significant change points in the SST evolution of the (sub)-tropics and high latitudes that potentially relate to changes in the WC. We find that the WC experienced a multifaceted evolution between the Late Pliocene and the Early Pleistocene with significant transitional steps at ~2.7 and ~2.1 - Ma. Our results suggest after the Late Pliocene, a pre-modern WC set in, which was characterized by a progressively strengthened Pacific Walker Cell alongside a weakened Indian Ocean Walker Cell. This change was potentially triggered by the constriction of the Indonesian seaway, an important transmitter between the Pacific and Indian Ocean. The ensuing mode of the WC intensified until ~2.1 Myr, when SST values around the global scale signalled a progressive strengthening of the Indian Walker Cell in phase with the progressive strengthening of the Pacific and Atlantic Cells. Our findings indicate that a shift from a pre-modern to a modern-like WC potentially only occurred during the mid-Pleistocene.

1. Introduction

The WC is the dominant atmospheric circulation pattern across the tropics consisting of east–west trending convection and subsidence cells along the equator that are characterized by large fluctuations on seasonal to multidecadal timescales (Bjerknes, 1966, 1969; Walker, 1923; Webster, 1983). In turn, the WC variability is directly coupled to changes in tropical SST of the Pacific, Indian and Atlantic Oceans (Lau and Yang, 2003; Webster, 1983). The seasonal variations of the WC are reflected as an east-west swaying of the large-scale circulation in the tropical atmosphere fostering intense rainfall in one region while other regions experience profound droughts (de Oliveira et al., 2018). However, its sphere of influence by far exceeds the tropical realm as WC

* Corresponding author.
E-mail address: kabothbahr@uni-potsdam.de (S. Kaboth-Bahr).

https://doi.org/10.1016/j.quascirev.2022.107529

fluctuations via Rossby and Kelvin waves propagate around the globe and can also manifest themselves in the climate variables SST and extension of sea-ice variability within the Arctic and Antarctic regions (Bodart and Bingham, 2019; Liu et al., 2004). Over the past twenty years, the WC has gained increasing interest also in the palaeoclimatic and palaeoceanographic communities due to the ongoing debate on the effectiveness of the tropics in modulating global climate change on orbital to millennial timescales (e.g. Beck et al., 2018; Martínez-Garcia et al., 2010; McClymont and Rosell-Melé, 2005; Molnar and Cane, 2002).

In particular, the role of the WC during the transition from the Late Pliocene towards the Early Pleistocene, one of the most profound climatic shifts of the Cenozoic era, has gathered significant interest. This transition is marked by the intensified growth of Northern Hemisphere ice sheets between 3.6 and 2.4 Myr (iNHG; Mudelsee and Raymo, 2005), and the onset of strong glacial-interglacial fluctuations that are characteristic for the Pleistocene epoch (Shackleton, 1987; Shackleton et al., 1984). Lines of arguments to explain this climate shift generally invoke atmospheric carbon dioxide and global temperature changes caused by tectonically driven gateway modifications and/or reduced heat transport by the Atlantic Ocean (Haug et al., 1999; Haug and Tiedemann, 1998; Keigwin, 1982; Raymo and Ruddiman, 1992). A serious hindrance to a strict testing of such arguments is the limited proxy data quality of past atmospheric carbon dioxide concentrations, that is, for time intervals that go further back than the currently longest ice core record (~0.8 M a) from the EPICA project (Lüthi et al., 2008). However, a distinct shift in the WC fostering an increased transport of heat and moisture via the atmosphere from the tropics into the high latitudes has also been proposed to explain the intensification of Northern hemisphere glaciation (Lawrence et al., 2006; Molnar and Cane, 2002). The onset of the modern WC between ~2.4 and 0.9 Myr (Etourneau et al., 2010; Liu et al., 2019; Martínez-Garcia et al., 2010; McClymont and Rosell-Melé, 2005; Ravelo et al., 2004; Singh et al., 2021; Trauth et al., 2009) has been linked to profound changes in the global heat budget including cooling in the North Pacific and South Atlantic (Lawrence et al., 2006; Martínez-Garcia et al., 2010; Zhang et al., 2014), tectonic modulation of the Indonesian Seaway (IS; Bahr et al., 2021; Bali et al., 2020; Cane and Molnar, 2001; Karas et al., 2009; Smith et al., 2020), as well as an increased northwards heat transport in the Atlantic Ocean (Bell et al., 2015). In addition, the WC changes, due to their profound impact in tropical precipitation, have also been invoked as a key player in the emergence and dispersion of early humans (e.g. Kaboth-Bahr et al., 2021; Maslin et al., 2014; Trauth et al., 2015, 2007).

Despite its potential significance on regional to global scales, a comprehensive analysis of the spatiotemporal evolution of the WC during the transition between the Late Pliocene and Early Pleistocene (3.5–1.5 Myr) remains elusive. This is due to the fact that previous studies (i) are usually based on a limited amount of proxy records (here assumed to be less than five), (ii) are often geographically restricted to the equatorial Pacific Ocean region, (iii) employ different SST reconstruction methods (generally the mostly utilized climate variable for WC assessment) carrying varying degrees of uncertainties, and (iv) did not fully employ state-of-the-art tools of statistical time series analysis. This all may have biased the determination of the onset of the WC and the assessment of its geographical scale of impact in previous studies.

Thus, in order to achieve a comprehensive understanding of the spatiotemporal evolution of the WC during the Late Pliocene to the Early Pleistocene (3.5–1.5 Myr), we analysed 30 globally distributed SST records covering the low and high latitudes. We applied a statistical change-point regression model to the selected time series to decipher (i) the onset of the WC, (ii) the spatiotemporal pattern of temperature change in the tropics related to WC changes, and (iii) the synchronicity of the temperature change between low and high latitudes. This paper provides a global perspective on, and a quantitative analysis of, the onset of modern WC changes, the underlying driving mechanism of its evolution and its concurrence with global climate events.

2. The modern and past Walker Circulation

The dominant component of the modern WC (Fig. 1) is the Pacific atmospheric cell, which in its mean state consists of easterly winds at the lower troposphere, westerly winds at the upper troposphere, rising motion over the western Pacific, and subsidence over the eastern Pacific (Bjerknes, 1969; Walker, 1923; Webster, 1983). Interconnected to the Pacific branch are the Walker Cells across the Indian and the Atlantic Oceans (Webster, 1983). The Indian Ocean cell is characterized by rising motion over the maritime continent in the east and subsidence over the western Indian Ocean, fuelling the lower tropospheric westerlies. Across the Atlantic Ocean, the raising motion is located off the coast of eastern Brazil in the east equatorial Atlantic and subsidence occurs over the west African continent, giving rise to weaker tropospheric easterlies (de Oliveira et al., 2018; Webster, 1983).

The WC possesses pronounced variability on seasonal to multidecadal timescales, which are expressed within a framework comprising the El Niño-Southern Oscillation (ENSO) with its end-members El Niño and La Niña, the Indian Ocean Dipole (IOD) with its positive and negative stage, and the Atlantic Equatorial Mode (AEM) characterized by Atlantic El Niño and La Niña conditions (Cane, 1998; Chang et al., 2006; Webster, 1983). During La Niña conditions (Fig. 1) and an enhanced Pacific WC, the prevailing intensified easterlies cause upwelling of cooler waters in the eastern equatorial Pacific and piling up of warmer waters in the western equatorial Pacific warm pool, where the warmest SSTs of the global ocean and strong atmospheric convection are found (van Oldenborgh et al., 2005). Under El Niño conditions, the WC across the Pacific Ocean weakens, the zone of atmospheric convection migrates eastwards, and the zonal SST gradient is reduced (de Oliveira et al., 2018). Through the propagation of Kelvin and Rossby waves, El Niño/La Niña conditions favour distinct responses in the Indian and Atlantic Oceans (Fig. 1; de Oliveira et al., 2018; Pausata et al., 2017). The El Niño-induced subsidence over the maritime continent (e.g., Indonesia; Fig. 1) leads to a weakening, or even a reversal, of the westerlies across the equatorial Indian Ocean, initiating pooling of warm water in its western part (positive IOD). As a consequence, eastern Africa experiences increasingly humid conditions due to the adjacent strong convection over the northwestern Indian Ocean, while extreme dry conditions prevail in western Australia (Fig. 1; Nicholson, 2017; Webster, 1983; Zhang et al., 2015). While El Niño is typically initiated during boreal winter over the Indo-Pacific realm, it incites a lagged response during the subsequent spring-summer period over the Atlantic Ocean, where intensified trade winds cause the development of a cold tongue of upwelling water along the western African shore (Fig. 1; Atlantic Niño; de Oliveira et al., 2018). In combination with the dominant subsidence in western Africa, the reduced evaporation over the cooled eastern equatorial Atlantic increases the aridity across southern Africa in boreal winter and, in addition, the Sahel Zone during boreal summer (Pausata et al., 2017). During La Niña conditions, the entire WC system reverses from the El Niño scenario leading to a negative IOD and an Atlantic La Niña development (Fig. 1; de Oliveira et al., 2018). These modes of the WC can lead to extreme weather conditions within the tropics and beyond. For instance, positive IOD events can cause large societal and economical losses, including severe haze problems in Indonesia

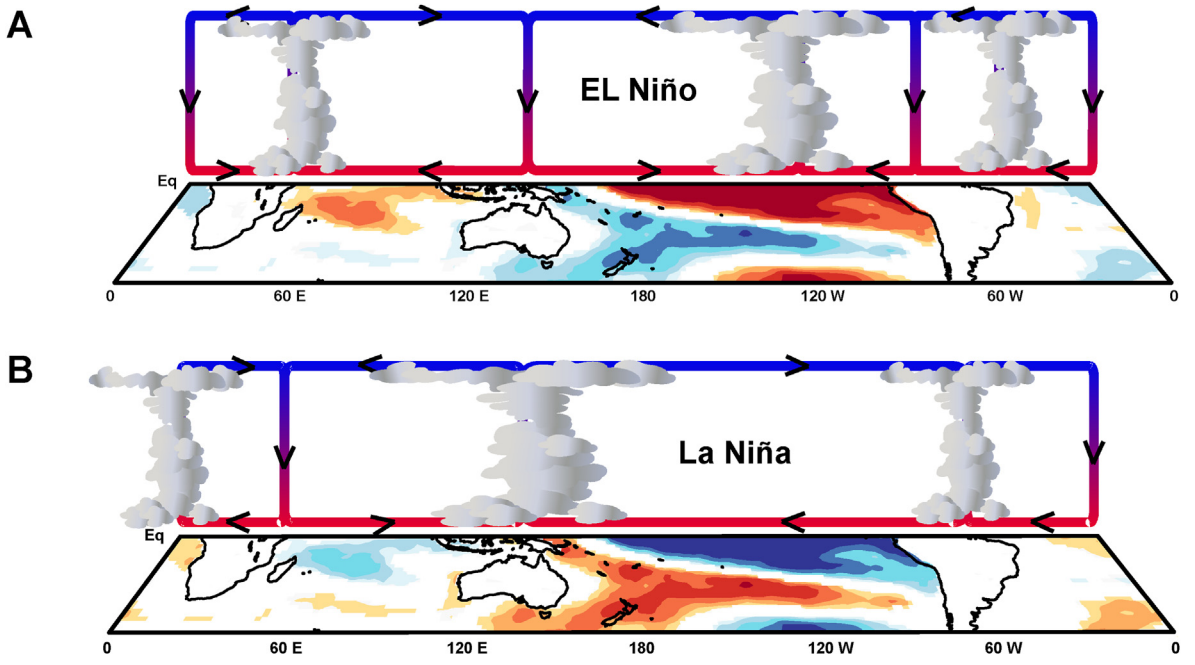

Fig. 1. Modern WC variability. (**A**) SST anomalies and resulting changes in tropical heating and convection (related to WC) under El Niño conditions; (**B**) SST anomalies and resulting changes in tropical heating and convection (related to WC) under La Niña conditions. Blue areas, cooling relative to normal conditions; red areas, warming relative to normal conditions; black arrows indicate atmospheric transport direction. Modified after Kaboth-Bahr et al. (2021). (For interpretation of the references to colour in this figure legend, the reader is referred to the Web version of this article.)

due to forest fires, exceptionally long lasting droughts in western Australia, and increased flooding in East Africa (Luo et al., 2008). In addition, El Niño conditions have been associated with thinning of Arctic sea ice (Liu et al., 2004), while western Antarctic ice shelves gain in their heights through intensified snowfall (Bodart and Bingham, 2019).

During the warm Pliocene (5.3–2.6 Ma), both meridional and zonal SST gradients across the Pacific Ocean were generally weak (Herbert et al., 2016; Liu et al., 2019), thus indicating a weak Pacific Ocean WC. With the progressive restriction of the Central American Seaway at around ~4.3 Ma, the eastern equatorial Pacific cold tongue developed first gradually and then at a faster pace during the iNHG (Bahr et al., 2021), then facilitated a strengthening of the zonal SST across the equatorial Pacific Ocean after ~4 Ma and, most likely, is linked to the intensification of the WC (Brierley et al., 2009; Tierney et al., 2019). During the time interval between ~4 and 3 Myr, the tectonic constriction of the Indonesian Seaway commenced, progressively increasing the sensitivity of the Indonesian Throughflow (ITF) to glacio-eustatic variability, and thus continuously reduce the inflow of relatively warm water from the southern Pacific Ocean (Auer et al., 2019; De Vleeschouwer et al., 2018; Petrick et al., 2019). At around ~3.3 Ma, proxy records document considerable cooling of the subsurface eastern Indian Ocean as well as the surface Leeuwin Current (Smith et al., 2020; Karas et al., 2009), which receives direct contributions from the ITF. During the early to mid-Pleistocene, a strengthening of the WC has been proposed for different dates ranging between ~2.4 and 0.9 Myr, which are based mostly on single-site analysis in the Indian Ocean for various proxy records (Berner et al., 2022; deMenocal, 2012; Etourneau et al., 2010; Lepre and Quinn, 2022; Liu et al., 2019; Martínez-Garcia et al., 2010; McClymont and Rosell-Melé, 2005; Ravelo et al., 2004; Singh et al., 2021; Trauth et al., 2009; van der Lubbe et al., 2021).

3. Material and methods

3.1. Study sites and site selection criteria

The selection of low latitude sites for the assessment of the WC followed several criteria: (i) geographical location between 30°N and 30°S – the direct influence sphere of the WC; (ii) time period between 3.5 and 1.5 Myr – argued to be the time interval of the onset of the modern WC; (iii) minimum temporal spacing of the proxy record of ~10 ka to allow a sufficient amount of data points for the statistical analysis; (iv) good age control for the time interval between 3.5 and 1.5 Myr; and (v) available SST-related proxy records. The latter is derived from varying methods such as (a) the oxygen isotopic composition ($\delta^{18}O_p$) of planktic foraminifera species *Globigerinoides ruber* (white or pink) and *Globigerinoides sacculifer*, (b) alkenone UK^{37} measurements, (c) Mg/Ca-palaeothermometry derived from planktic foraminifera species *G. ruber* or *G. sacculifer*, and (d) membrane lipids of mesophilic marine thaumarchaeota (TEX_{86}). The selection of SST proxy records for our analysis follows the reasoning that SST changes in the tropics are under modern climate conditions predominantly driven by WC changes, and that a similar linkage has also been proposed for the geological past (see Section 2 for more details).

For the low latitude SST analysis, a number of 30 proxy records from 27 different sites were selected following the above outlined criteria. These include 11 coarse-resolution (average temporal spacing above 10 ka) and 19 high-resolution (less than or equal to 10 ka) proxy records (Table 1), 10 records of $\delta^{18}O_p$, 16 records of SST reconstructions based on alkenone UK^{37} measurements, 2 records of Mg/Ca-palaeothermometry and 2 records based on TEX_{86} palaeothermometry. At Sites ODP 722, 806 and 999 both, $\delta^{18}O_p$ as well as SST records from UK^{37} and Mg/Ca-palaeothermometry, for the studied time interval were available thus allowing for simultaneous analysis of both signals for these three sites.

As strong interferences between high latitude climate change

Table 1
Selected proxy records for the time interval from 3.5 to 1.5 Myr. LAT = Latitude; LON = Longitude; Depth = water depth; Res = temporal resolution; SR = sedimentation rate.

Site	LAT	LON	Depth (m)	Res (kyr)	SR (cm/kyr)	Reference	Interval (Myr)
Sea surface temperature (SST)							
ODP 662	1°23′S	11°44′W	3824	2.3	30	Herbert et al. (2016)	1.5–3.5
ODP 722	16°37′N	59°47′E	2033	1.9	32	Herbert et al. (2010)	1.5–3.3
ODP 806	0°19′N	159°22′E	2520	9.1	3.3	O'Brien et al. (2014)	1.5–3.5
ODP 846	3°05′S	90°49′W	3296	5.4	27.2	Herbert et al. (2016)	1.5–3.5
ODP 850	1°17′N	110°31′W	3786	~150	1.9	Herbert et al. (2016)	1.5–3.5
ODP 882	50°21′N	167°35′E	3255	6.6	9.0	Haug (1996)	1.5–3.5
ODP 982	57°30′N	15°51′W	1134	4.1	2.7	Lawrence et al. (2009)	1.5–3.5
ODP 999	12°44′N	78°44′W	2828	~120	3.1	O'Brien et al. (2014)	1.5–3.2
ODP 1010	29°57′N	118°05′W	3466	67	1.8	O'Brien et al. (2014)	1.5–3.5
ODP 1082	21°05′S	11°49′E	1279	4.4	10.9	Etourneau et al. (2009)	1.5–3.5
ODP 1084	25°30′S	13°01′W	1991	~200	1.8	Farmer et al. (2005)	1.5–3.5
ODP 1088	41°08′S	13°33′E	2081	~48	0.7	Herbert et al. (2016)	1.5–3.5
ODP 1090	42°54′S	8°53′E	3699	4.0	1.7	Martínez-Garcia et al. (2010)	1.5–3.5
ODP 1125	42°32′S	178°9′W	1365	~36	6.3	Herbert et al. (2016)	1.5–3.5
ODP 1143	9°21′N	113°17′E	2771	2.5	24.1	Li et al. (2011)	1.5–3.5
ODP 1239	0°40′S	82°05′W	1414	3.5	10.4	Etourneau et al. (2010)	1.5–3.1
ODP 1241	5°50′N	86°26′W	2026	~100	3.1	Herbert et al. (2016)	1.5–3.5
U1338	2°30′N	117°58′W	4210	~150	2.8	Liu et al. (2019)	1.5–3.3
U1460	27°22′S	112°55′E	215	10	23.3	Petrick et al. (2019)	1.5–3.5
U1463	18°57′S	117°37′E	145	5.5	11.6	Smith et al. (2020)	1.5–3.3
Planktic stable oxygen isotopes ($\delta^{18}O_p$)							
DSDP 586	0°30′S	158°30′E	2218	2.8	56.5	Whitman and Berger (1992)	1.5–3.5
DSDP 590	−31°10′S	163°21′E	1299	~100	5.3	Whitman and Berger (1992)	1.6–3.5
ODP 625	28°50′N	87°10′W	889	3.7	4.3	Joyce et al. (1990)	1.5–3.5
ODP 709	3°54′S	60°33′E	3047	10	1.1	Shackleton and Hall (1990)	1.5–3.5
ODP 722	16°37′N	59°48′E	2028	2.7	12.1	Murray and Prell (1991)	1.5–3.5
ODP 758	5°23′N	90°21′E	2925	1.3	7.1	Farrell and Janecek (1991)	1.5–3.5
ODP 806	0°19′N	159°22′E	2520	3.3	3.5	Jansen et al. (1993)	1.5–3.5
ODP 851	2°46′S	110°34′W	3760	1.9	5.2	Cannariato and Ravelo (1997)	1.5–3.5
ODP 999	12°44′N	78°44′W	2828	3	3.2	Haug et al. (2001)	1.6–3.5
ODP 1148	18°50′N	116°34′E	3294	2.5	9.8	Cheng et al. (2004)	1.5–3.5

and the evolution of the WC during the Plio-Pleistocene have been previously suggested (Lawrence et al., 2006; Martínez-Garcia et al., 2010; Zhang et al., 2014), we also assessed the SST evolution of selected sites from the high latitudes of the southern and northern hemisphere. The criteria for the selection of high latitude sites followed the same criteria stated for the low latitude sites (i.e., points ii, iii, iv, and v) with the only exception that the referenced high latitude sites needed to be geographically positioned either north of 50°N or south of 40°S. Following this outline for the high latitude analysis, a total number of 5 SST proxy records from 5 different sites were utilized. These include 3 high-resolution records (less than or equal to 10 ka) and 2 low-resolution records (average temporal spacing above 10 ka) proxy records (Table 1). The SST evolution from all utilized high-latitude sites (ODP 882, 982, 1088, 1090, 1125) is based on alkenone UK^{37} measurements.

3.2. Method overview of proxy records selected in this study

Accurately quantifying SSTs during Earth's history is critical for understanding a range of key climate processes, such as climate sensitivity, polar amplification as well as the evolution of the earth-spanning wind systems such as the tropical WC. In the following, a brief summary of the methods and their potential limitations for the SST proxy records utilized in this study is provided. However, readers are referred to the cited references for each method for an in-depth assessment of the individual methods.

The utilization of oxygen isotope ratios derived from planktic foraminifera test as a palaeothermometer is based on the principle of thermodynamic fractionation between ^{16}O and ^{18}O that occurs during calcite precipitation (Urey, 1947). In contrast, Mg/Ca-palaeothermometry follows the rationale that the incorporation of the Mg^{2+} instead of the Ca^{2+} ion into foraminiferal calcite is influenced by the temperature of the surrounding seawater during growth (Nürnberg et al., 1996). In addition, the ratio of di to di-plus tri-unsaturated long-chain C_{37} methyl ketones (alkenones) synthesized by certain prymnesiophyte microalgae has been shown to vary linearly with the seawater temperature in which the organisms grow (Prahl et al., 1988). Although these palaeothermometers are widely applied, each method carries distinct uncertainty levels, a fact that introduces noise into the resulting SST data. For instance, $\delta^{18}O_p$ reflects both, temperature changes as well as changes in the oxygen isotopic composition of the seawater ($\delta^{18}O_{sw}$) in which the foraminifera shell was calcified (i.e., the ice volume and salinity effects; see Shackleton, 1987 and Ravelo and Hillaire-Marcel, 2007). If $\delta^{18}O_{sw}$ is known (as is the case for the analysed time frame), the uncertainty (i.e., standard deviation) of temperatures estimates based on $\delta^{18}O_p$ is in the range of 0.5–1.0 °C (e.g. Lea, 2014; Ravelo and Hillaire-Marcel, 2007). However, unconstrained changes in $\delta^{18}O_{sw}$ can carry substantial uncertainties for palaeotemperatures derived from $\delta^{18}O_p$. The average standard deviation of the Mg/Ca-palaeothermometry method is approximately 1 °C, however, this method is particularly sensitive to carbonate dissolution effects, to carbonate ion effects as well as to secular Mg/Ca-variations of the foraminiferal test; this all may cause an underestimation of SSTs by several degrees (e.g. Lea, 2014; Regenberg et al., 2006). Alkenone-derived SSTs carry typical standard deviations of ~1.5 °C, but have been demonstrated to be sensitive to algae-species variations and seasonally biased growth (e.g. Herbert et al., 1998; Lea, 2014). Lastly, the TetraEther indeX of 86 carbons (TEX_{86}) is based on the distribution of isoprenoidal glycerol dialkyl glycerol tetraethers (isoGDGTs) in marine (and lake) sediments (Schouten et al., 2002; Inglis and Tierney, 2020). Within marine environments, isoGDGTs are thought to be mainly derived from ammonia-oxidising Thaumarchaeota that inhabit both the surface ocean and mesopelagic zone (Church et al., 2010; Schouten et al., 2002; Villanueva et al., 2015; Wuchter et al., 2004). The TEX_{86} paleothermometer can be

influenced by thermal maturation, exogenous sources of GDGTs (i.e., those other than marine Thaumarchaeota), by seasonal production (and export) of GDGTs and additionally by physiological and environmental controls (Inglis and Tierney, 2020). However, it should be noted that recent findings have argued that TEX_{86} in the equatorial Pacific region might represent long-term changes in thermocline conditions across Plio-Pleistocene rather than SST variability (Ford et al., 2015; Hertzberg et al., 2016). TEX_{86}-derived SSTs carry typical standard deviations of between 1 and 2 °C, depending on the calibrations used (Inglis and Tierney, 2020).

3.3. Chronostratigraphic alignment of sites

Prior to time series analysis, we assessed the age models of the selected proxy records and their uncertainties (Table 1). This is necessary to ensure that all analysed proxy records adhere within error margins to a common chronostratigraphic framework during the interval from 3.5 to 1.5 Myr. This is to ensure that the deviations in the determined temporal offsets among change-point times from individual records can likely not be attributed to differences in the applied chronologies.

The age model constrains of the majority of selected sites (22 records) is derived from tuning the $\delta^{18}O$ record obtained from benthic foraminifera species or the SST proxy record from site U1460 to the global benthic $\delta^{18}O$ stack LR04 (Lisiecki and Raymo, 2005). This provides age uncertainties in the range of 4–20 kyr for the Late Pleistocene to Late Pliocene. The chronostratigraphy of Site U1338 was achieved via orbital tuning to different insolation (e.g. June 21st summer insolation at 65°N or 30°N) or other Earth's orbital target parameters (e.g., obliquity). These orbital tunings have phase shifts relative to the LR04-based age models of less than 10 kyr during the investigated time frame (Lisiecki and Raymo, 2005). For the proxy records from Sites DSDP 586 and 590, ODP 625 and 709, the age model is based on biostratigraphic or magnetostratigraphic tie points (see respective references in Table 1 for more details), which are associated with a greater age uncertainty than derived through benthic $\delta^{18}O$ to LR04 matching and/or orbital tuning methods. Generally, the magnetostratigraphic dates exhibit an excellent agreement with astronomically tuned dates with an average error of ~25 ka (Mudelsee and Raymo, 2005), while biostratigraphic dates are likely less accurate because of stratigraphic uncertainties and site-specific dependences of the habitats.

3.4. Statistical change-point analysis

Change points are a manifestation of abruptness in a time series model. Such abrupt changes may represent transitions that occur between states. Thus, a change-point analysis is performed on a time series in order to detect whether any abrupt changes have occurred and temporally constrain these changes. In the simplest of cases, a one-change-point system, the change point divides a time series into two segments where each segment has its own statistical properties (mean, variance, etc.). Thus, the change point is located where the underlying characteristics change abruptly. Based on the available insight on the evolution of the WC during the Plio-Pleistocene (see Section 2 for more details), the onset of the modern WC has been attributed to a distinct change point at around ~2 Ma (Berner et al., 2022; deMenocal, 2012; Etourneau et al., 2010; Lepre et al., 2021; Liu et al., 2019; Martínez-Garcia et al., 2010; McClymont and Rosell-Melé, 2005; Ravelo et al., 2004; Singh et al., 2021; Trauth et al., 2009; van der Lubbe et al., 2021). To assess the validity of this dominant change of the WC during the early Pleistocene, we determined the dominant change points of the selected SST proxy records during the studied time interval from 3.5 to 1.5 Myr – assuming that surface temperature changes in the tropics are predominantly driven by WC changes. For the change point analysis, one requires only the relative change of the temperature evolution recorded for each individual proxy records used, not their absolute temperature amplitude change. We assume that each proxy record utilized in this study represents a surface water temperature signal of a specific region following the statement made in their respective references (see Table 1). As our statistical assessment does not require an assessment of the absolute temperature change between the selected proxy records, a correction between the different utilized proxy records (e.g., inter-proxy corrections between TEX_{86} and UK^{37} or Mg/Ca-ratio based SST reconstructions) is not necessary prior to the change point analysis. In other words, the line of interpretation in the present manuscript is tied to the change-point time estimates, which are unaffected by proxy calibration issues.

For the change point analysis, we employed the statistical tool of ramp function regression (Mudelsee, 2000). The ramp is a piecewise-linear model with four parameters. It describes the trend as a constant level (x_1) up to the first change-point time (t_1), then a linear change to the second change-point time (t_2), and then again as a constant level (x_2). The parameters x_1 and x_2 are estimated by means of minimizing an ordinary least-squares sum (Mudelsee, 2000). Since the ramp is not differentiable with respect to time, the search for the best-fit change-point times (parameters t_1 and t_2) is performed in a brute-force manner, that is, (i) all possible combinations for t_1–t_2 are taken from the set of time values, (ii) the constraint $t_1 < t_2$ is imposed and (iii), that solution is retained which has an overall minimum least-squares sum. The standard errors for the four estimated parameters are obtained by means of moving block bootstrap resampling (Mudelsee, 2014), where the ramp fitting procedure is repeated 2000 times on the resampled time series. The resampling consists in adding random time-blocks of fit residuals (i.e., data minus fit) to the fitted ramp (Künsch, 1989); this data-driven procedure does not require distributional assumptions (e.g., a Gaussian shape of the distribution of the residuals), and it also takes autocorrelation or persistence into account since the block length is determined via the persistence time (Mudelsee, 2002) of the fit residuals. The ramp fit function is given by

$$x_{\mathrm{fit}}(t) = \begin{cases} x_1 \text{ for } t \le t_1, \\ x_1 + (t - t_1)(x_2 - x_1)/(t_2 - t_1) \text{ for } t_1 < t \le t_2, \\ x_2 \text{ for } t > t_2. \end{cases}$$

The standard error for a change-point time is then given by the standard deviation over the 2000 copies (for t_1 or t_2). This computing-intensive estimation procedure is feasible for data sizes up to millions on today's computers, it has been validated in Monte Carlo experiments with artificial data (Mudelsee, 2014), and it has found entrance into different research disciplines ranging from astronomy to zoology. The ramp function regression is implemented in the FORTRAN 77 program RAMPFIT available for download at https://www.manfredmudelsee.com.

The analysis of the SST and $\delta^{18}O_p$ time series revealed two positive intermediate results. First, for each parameter, we found that estimation bias is negligible since the median of the 2000 simulated parameter estimates is rather close to the original fit result. Second, for the change-point time parameters, we found that the standard errors (Table 2) are clearly larger than (i) the timescale uncertainties (Section 2.2), and (ii) the spacing at around the change-points. That means, no adaptation of the regression procedure by means of bias correction, timescale simulations or a fine search (between the sampling times) was necessary.

For a number of analysed records (6 from 30), the ramp fitting procedure resulted in boundary solutions, where t_1 is on the left boundary (1.5 Myr), t_2 on the right boundary (3.5 Myr), or both

Table 2
Estimated change point times (t_1) for the selected proxy records from 3.5 to 1.5 Myr. LAT, latitude; LON, longitude; t_1, change-point time (Myr); σ_{t1}, uncertainty of t_1 (Ma). Comments may state that the number of data points is insufficient for a highly confident statistical estimation (Mudelsee, 2014) or that the estimate of t_1 is at the time interval boundary.

Site	LON	LAT	Proxy	t_1(Ma)	σ_{t1} (Ma)	Comment
DSDP 590	0°30′S	158°30′E	$\delta^{18}O_p$	2.660	0.357	
DSDP 586	31°10′S	163°21′E	$\delta^{18}O_p$	2.603	0.208	
ODP 625	28°50′N	87°10′W	$\delta^{18}O_p$	1.989	0.376	
ODP 662	1°23′S	11°44′W	SST	2.249	0.108	
ODP 709	3°54′S	60°33′E	$\delta^{18}O_p$	2.946	0.234	
ODP 722	16°37′N	59°48′E	$\delta^{18}O_p$	2.296	0.198	
ODP 722	16°37′N	59°48′E	SST	2.162	0.079	
ODP 758	5°23′N	90°21′E	$\delta^{18}O_p$	2.684	0.099	
ODP 806	0°19′N	159°22′E	$\delta^{18}O_p$	2.754	0.157	
ODP 806	0°19′N	159°22′E	SST	3.000	0.132	
ODP 846	3°05′S	90°49′W	SST	2.090	0.248	
ODP 850	1°17′N	110°31′W	SST	1.511	0.274	Too few data points; Boundary solution
ODP 851	2°46′S	110°34′W	$\delta^{18}O_p$	2.476	0.249	
ODP 882	50°21′N	167°35′E	SST	2.723	0.310	
ODP 982	57°30′N	15°51′W	SST	2.481	0.188	
ODP 999	12°44′N	78°44′W	SST	2.110	0.308	Too few data points
ODP 999	12°44′N	78°44′W	$\delta^{18}O_p$	2.516	0.206	
ODP 1010	29°57′N	118°05′W	SST	1.552	0.290	Boundary solution
ODP 1082	21°05′S	11°49′E	SST	2.200	0.103	
ODP 1084	25°30′S	13°01′W	SST	1.667	0.394	Too few data points
ODP 1088	41°08′S	13°33′E	SST	3.227	0.373	
ODP 1090	42°54′S	8°53′E	$\delta^{18}O_p$	2.300	0.293	
ODP 1125	42°32′S	178°9′W	SST	2.335	0.406	
ODP 1143	9°21′N	113°17′E	SST	1.749	0.178	
ODP 1148	18°50′N	116°34′E	$\delta^{18}O_p$	1.702	0.407	
ODP 1239	0°40′S	82°05′W	SST	1.798	0.170	
ODP 1241	5°50′N	86°26′W	SST	1.995	0.344	
U1338	2°30′N	117°58′W	SST	1.578	0.037	
U1460	27°22′S	112°55′E	SST	2.124	0.309	Too few data points
U1463	18°57′S	117°37′E	SST	1.507	0.275	Boundary solution

(Figs. 2 and 3). In such a situation, it is still possible to perform a meaningful interpretation of the "other" change point, which does not sit at the boundary.

As regards to the selected degree of complexity of the ramp (with four parameters) as a model of a climate transition, we choose to apply Ockham's Razor in the form given by Isaac (Newton, 1687, p. 402 therein): "Keep things simple. But not too simple!" On one hand, the simple straight-line model (with two parameters) has no change point and therefore is unsuited. On the other, investing more parameters than four (in order to describe multiple-change points) may render a model too complex – resulting in estimations which may be too difficult to interpret, and the estimation procedure may land in several local least-squares minima (statisticians speak of the danger of "overfitting"). We therefore believe that under Ockham's Razor, the ramp constitutes a sound degree of model complexity.

4. Results

We observe that the estimated change-point times lie between 1.55 and 3.33 Myr (Table 2; Figs. 2–4). The earliest change points (before ~2.7 Ma) can be observed at Sites ODP 709 (2.94 ± 0.23 Ma), 806 (3.00 ± 0.13 Ma), 882 (3.72 ± 0.31 Ma) and 1088 (3.22 ± 0.37 Ma). The latest change points (after 1.7 Ma) are associated with Sites ODP 850 (1.51 ± 0.27 Ma), 1010 (1.55 ± 0.29 Ma), 1084 (1.66 ± 0.39 Ma) and U1460 (1.57 ± 0.03 Ma).

In case of Sites ODP 850, 999, 1010, and U1338, U1463, however, the detected change points are considered as less reliable due to the low number of data points and/or the lack of discernible change within the search boundaries of the ramp fit (Table 2). However, we continued to include these sites in our discussion to provide the widest possible geographical and methodological coverage for each assessed region.

The combined analysis of SST and $\delta^{18}O_p$ at Sites ODP 806 ($\delta^{18}O_p$: 2.75 ± 0.15 Ma; SST: 3.00 ± 0.13 Ma), 722 ($\delta^{18}O_p$: 2.29 ± 0.19 Ma; SST: 2.16 ± 0.07 Ma) and 999 ($\delta^{18}O_p$: 2.51 ± 0.20 Ma; SST: 2.11 ± 0.30 Ma) show within the uncertainty ranges of determined individual change points a similar behaviour for the two proxy variables (Table 2; Fig. 4). This suggests that $\delta^{18}O_p$ changes at these sites were in phase to SST changes derived from alternative methods (e.g. alkenone- or Mg/Ca-palaeothermometry) within the same sample. This suggests that the long-term trends observed in $\delta^{18}O_p$ during the studied time interval are strongly related to SST changes with effects derived from $\delta^{18}O_{sw}$ negligible for our analysis, and thus underscore their utilization for the assessment of WC changes along with the SST records.

In addition to the change point analysis, we also visually assessed the SST evolution trend following the calculated change point which can be classified into three categories: (i) a persistent SST warming of the post change point time interval relative to the pre change point time interval (e.g., Sites ODP 709, 882 or 1088; Figs. 2 and 3), (ii) a persistent SST cooling of the post change point time interval relative to the pre change point time interval (e.g. Site ODP 850, 1010 or U1460; Figs. 2 and 3), and (iii) a persistent stabilization of the SST on a colder background level of the post change point time interval relative to the pre change point time interval (e.g., Sites ODP 758, 847, 882, 999 etc.; Figs. 2 and 3).

5. Discussion

5.1. Spatiotemporal patterns of SST changes between 1.5 and 3.5 Myr

Focusing first on the analysed low latitude SST records (see Section 3.1 for details; Table 1; Figs. 4 and 5), we find that the calculated change points range widely between ~3.0 Myr (ODP 806)

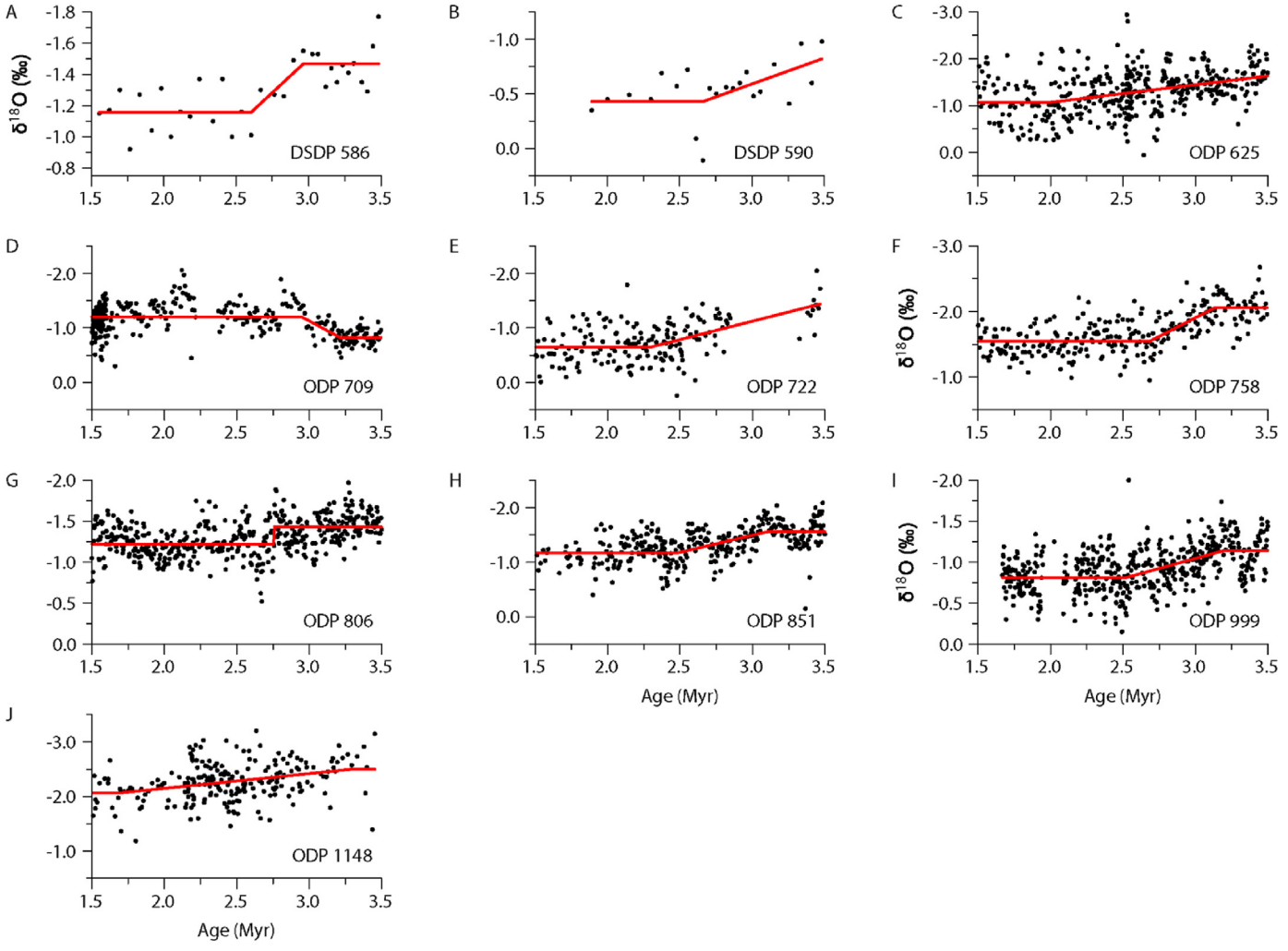

Fig. 2. Statistical change-point regression results based on the utilized (**A-J**) $^{18}O_p$ records (Tables 1 and 2). The fitted ramp regression curve is indicated by a red line. Original data points are shown as black dots. (For interpretation of the references to colour in this figure legend, the reader is referred to the Web version of this article.)

to ~1.5 Myr (e.g., Site U1460) between sites (Fig. 4). Interestingly, we can identify two distinct spatiotemporal patterns with change points clustering between 3.2 and 2.6 Myr (median change point of ~2.7 Ma) and 1.6–2.4 Myr (median change point of ~2.1 Ma) (Fig. 5).

The first cluster with a median change point at ~2.7 Ma pertains to sites located in the western tropical and subtropical Pacific Ocean (DSDP 586, DSDP 590 and ODP 806), as well as eastern and western equatorial Indian Ocean (ODP 709 and ODP 758). The median change point age of ~2.7 Ma signals a distinct and early change in the temperature evolution of the tropical and subtropical regions in specifically the western equatorial Pacific and across the equatorial Indian Ocean during the Plio-Pleistocene transition (Figs. 4 and 5). In contrast, sites pertaining to the median change point of ~2.1 Ma encompass the eastern equatorial Pacific (DSDP 590, DSDP 591, ODP 846, ODP 1010, U1338, U1239 and U1241), the Gulf of Mexico/Caribbean region (ODP 625 and ODP 999), the tropical to subtropical South Atlantic (ODP 662, ODP 1082 and ODP 1084) and as well the northwest (ODP 722) and southeast (U1460 and U1463) Indian Ocean. The ~2.1 Ma date temporally aligns with the early Pleistocene, and follows strongly previous estimates of WC changes during the Plio-Pleistocene time frame (e.g., Berner et al., 2022; Trauth et al., 2009; van der Lubbe et al., 2021, Figs. 4 and 5). Notably, the observed median temporal offset between both spatiotemporal clusters is ~0.65 Ma, and thus roughly twice the uncertainty of the individual change points (Table 2), and even larger than individual chronological uncertainties. Hence, this argues for the robustness of these two spatiotemporal clusters, and strongly suggests that the SST evolution of the low latitudes Pacific, Indian and Atlantic Oceans was neither temporally nor spatially uniform during the studied time interval between 3.5 and 1.5 Myr. Assuming that the SST evolution of the low latitudes is predominately driven by the WC, as is the case under modern climate background conditions and has been proposed to be the case since the early Pliocene (see Section 2 for more details), this also suggests that the WC evolution was most likely spatiotemporally variable during the Plio-Pleistocene. While previous assessments of WC changes from the late Pliocene towards the late Pleistocene focused primarily on an abrupt change around ~2 Ma, our results rather indicate that a distinct, older precursor in WC change occurred already at ~2.7 Ma, although this was limited to certain oceanic regions in the Pacific and Indian Oceans.

Secondly, we now include the change points from the analysed high latitude sites into our assessment, and we find a non-uniform spatiotemporal pattern of the high latitude temperature evolution similar to the low latitude sites. In detail, the northwestern Pacific (ODP 882) and South Atlantic (ODP 1088) show a change point at ~2.7 Ma and ~3.2 Ma, respectively (Figs. 4 and 5). This would, within the error margin of the age models, temporally align with the first

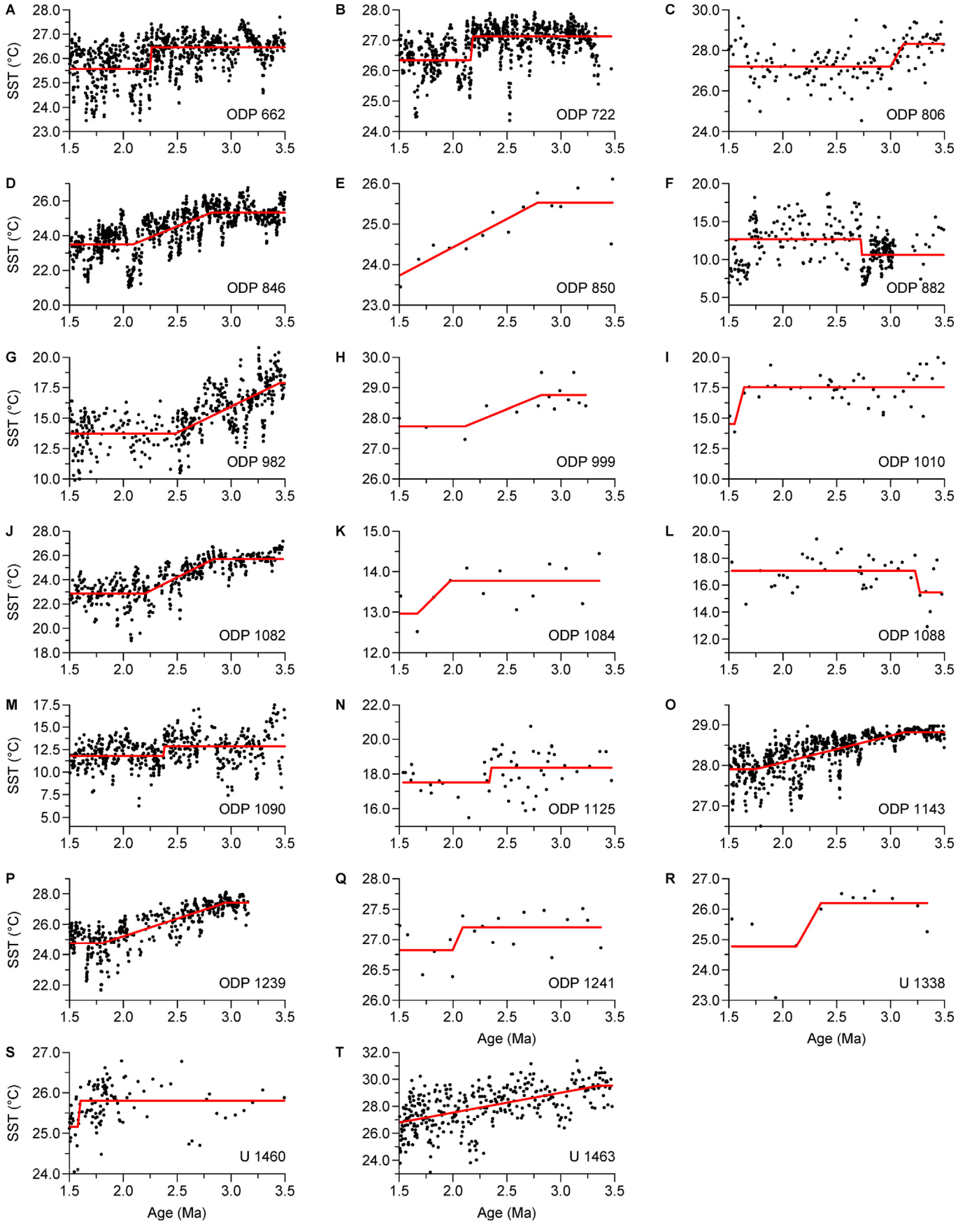

Fig. 3. Statistical change-point regression results based on the utilized (**A-T**) SST records (Tables 1 and 2). The fitted ramp regression curve is indicated by a red line. Original data points are shown as black dots. (For interpretation of the references to colour in this figure legend, the reader is referred to the Web version of this article.)

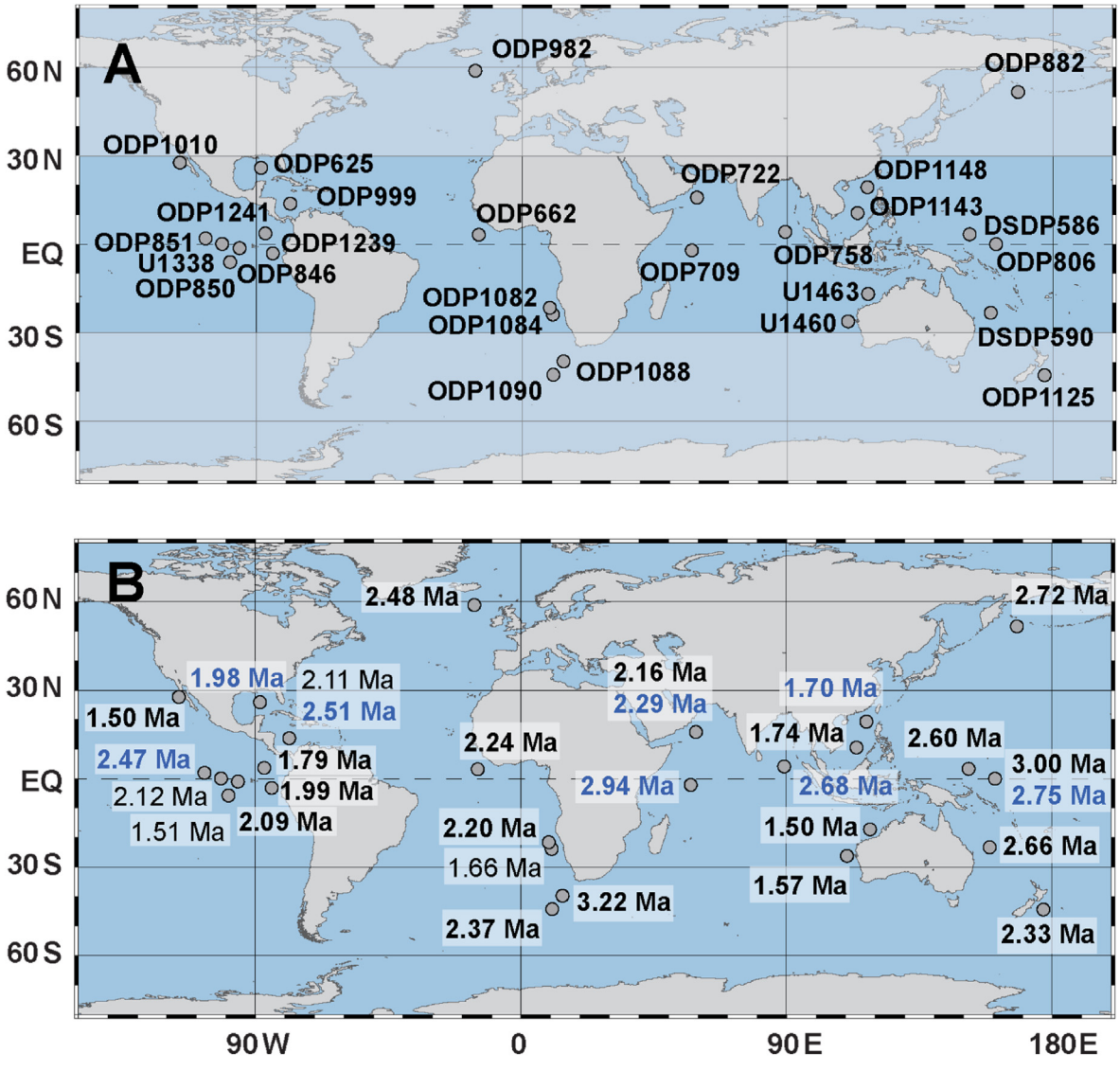

Fig. 4. Geographical overview of sites (**A**) and their calculated change points (**B**) in million years before present (Ma). Blue numbers: based on $\delta^{18}O_p$; black numbers: based on SST; bold type: high confidence level of estimated change point (Table 2); light type: low confidence level of estimated change point (see Table 2). (For interpretation of the references to colour in this figure legend, the reader is referred to the Web version of this article.)

cluster of the low latitude SST sites that are characterized by a median change point of ~2.7 Ma. In contrast, the North Atlantic (ODP 982), the South Pacific (ODP 1125) and an additional site from the South Atlantic (ODP 1090) all show change points between ~2.4 and ~2.3 Myr (Figs. 4 and 5), an observation that seems in closer temporal alignment with the median change point of ~2.1 Ma for the second cluster of the low latitude sites. Thus, both determined dominant change points at ~2.7 Ma and ~2.1 Ma are seemingly associated with a distinct array of low- and high-latitude sites, and thus do not substantiate a clear temporal or regional separation between high and low latitudes as previously proposed (Figs. 4 and 5). This also implies that at ~2.7 and ~2.1 Ma, specific regions of the low- and high-latitude regions did change quasi-synchronously (within the error margin of the individual change–point estimates), while other low- and high-latitude regions did not echo this temperature evolution. Notably, this finding aligns with previous studies arguing for a strong connectivity between low- and high-latitude climatic change during the Plio-Pleistocene and the Early to Middle Pleistocene (Lawrence et al., 2006; McClymont and Rosell-Melé, 2005), while opposing findings arguing that, for example, during the Plio-to-Pleistocene transition the high latitude experienced profound climatic change unaccompanied by a similar distinct change in the low latitudes (Martínez-Garcia et al., 2010).

At first glance, the resulting spatiotemporal pattern of SST changes during the Plio-Pleistocene transition and the early Pleistocene seems enigmatic. However, we argue that this pattern could provide crucial insights into the potentially multi-phased history of the WC during the studied time interval.

5.2. The evolution of the Walker Circulation between 3.5 and 1.5 Myr

For the next step in our discussion detailing the potential multifaceted history of the WC from the late Pliocene towards the early Pleistocene, we not only assessed the change points from each individual site but also considered the temperature trend of each utilized proxy record after the calculated change point (post-change-point trend) relative to its trend prior to the change point

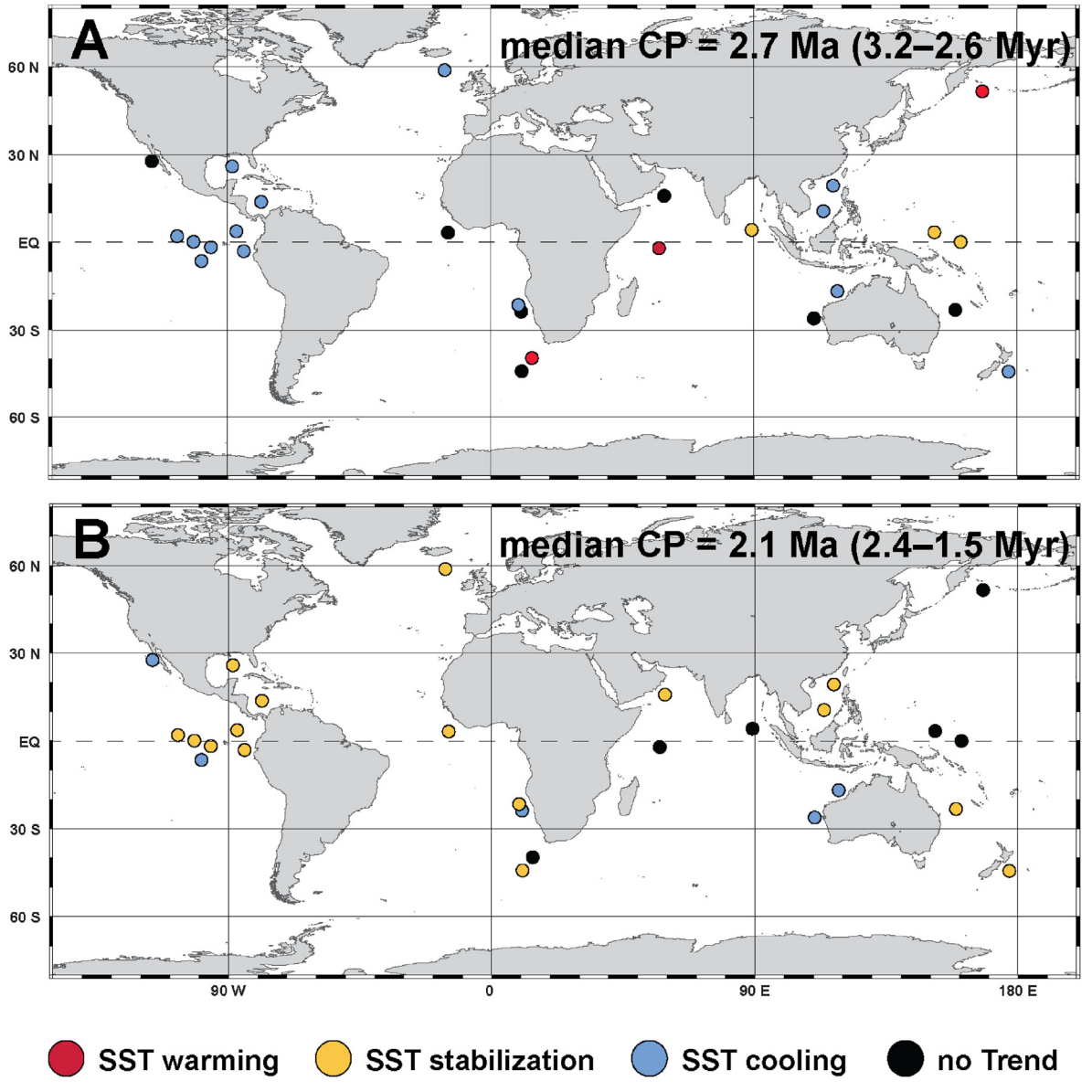

Fig. 5. Sign of change in the SST records of the selected sites for the time intervals between (**A**) 3.2 to 2.6 Myr and (**B**) 2.4 to 1. 5Myr. Red dots: SST warming; blue dots: SST cooling; orange dots: SST stabilization after cooling; black dots: no statistically significant SST trend. (For interpretation of the references to colour in this figure legend, the reader is referred to the Web version of this article.)

(pre-change-point trend).

The first phase encompasses the time interval between 3.5 Ma until the first dominant change point at ~2.7 Ma (Figs. 5 and 6). This interval is best described as the late Pliocene backdrop conditions characterized by warm SST conditions in the eastern as well western equatorial Pacific Ocean (Herbert et al., 2016; Liu et al., 2019), giving rise to a weakened meridional temperature gradient. A weakened meridional SST gradient between eastern and western equatorial pacific is symptomatic for a weakened WC under proposed prevalent El Niño-like conditions (e.g., Fedorov et al., 2006; Haywood et al., 2007; Wara et al., 2005, Watanabe et al., 2011; Zhang et al., 2014). In contrast, the Indian Ocean during this time period was most likely characterized by cooler western equatorial temperature relative to the eastern equatorial Indian Ocean (e.g., Karas et al., 2009), giving rise to an increased meridional SST gradient, which indicates a strengthened WC over the Indian Ocean (Figs. 5 and 6). At ~2.7 Ma, we find that (i) a sea surface warming experienced at sites ODP 709, 882 and 1088, which brought local SSTs above the Late Pliocene temperature levels, and (ii) a halt and stabilization of the initiated late Pliocene cooling trend at sites DSDP 586, DSDP 590, ODP 758 and 806 (Fig. 5). At the same time, the SST records from the equatorial eastern and southern Pacific Ocean, the South China Sea, and the North Atlantic show a continued cooling trend across the Plio-to-Pleistocene transition, while temperature in the South Atlantic, northwest and southeast Indian Ocean shows no discernible long-term changes during this time period (Fig. 5). This provides a distinct east-west trending SST pattern across the equatorial Pacific and Indian Ocean – with the eastern equatorial Pacific becoming cooler than the western Pacific Ocean, while the western equatorial Indian Ocean experiencing a distinct warming trend opposing cooling in the eastern Indian Ocean (Figs. 4–6). Interestingly, this SST pattern across both, the Pacific and Indian Ocean basins, resembles SST patterns that can be observed during modern La Niña

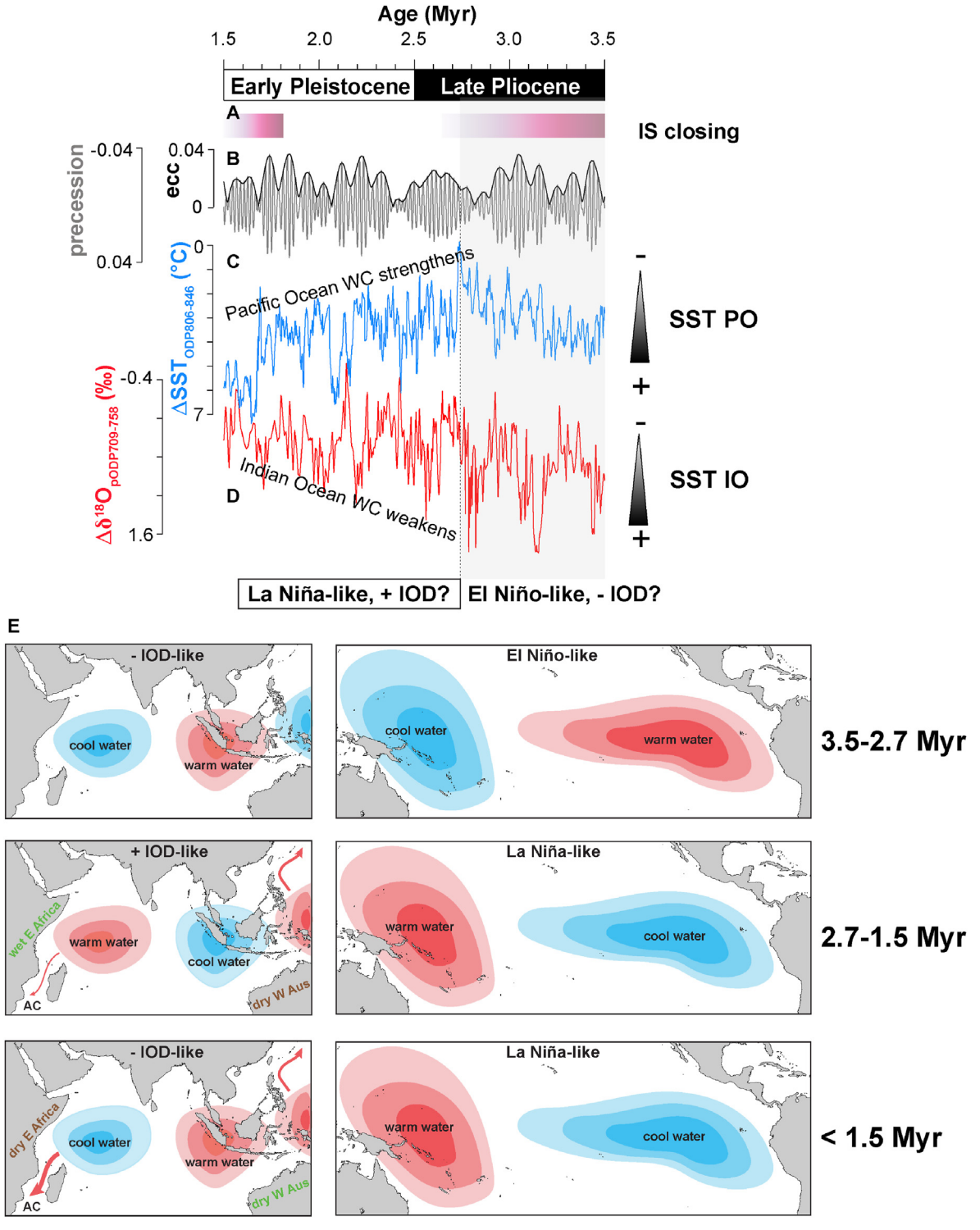

Fig. 6. Evolution of the WC during the studied time interval from 3.5 to 1.5 Myr. (**A**) Phases of constriction of the IS (Karas et al., 2009; Smith et al., 2020); (**B**) orbital eccentricity (ecc; black line) and precession (grey line) after Laskar et al. (2004); (**C**) SST gradient (ΔSST) between Sites ODP 806 (O'Brien et al., 2014) and ODP 846 (Herbert et al., 2016); (**D**) stable oxygen isotope gradient (Δ $^{18}O_p$) from Sites ODP 709 (Shackleton and Hall, 1990) and ODP 758 (Farrell and Janecek, 1991). (**E**) Schematic drawing of inferred SST changes across the Indian and Pacific Ocean during the three discussed main phases 3.5–2.7 Myr, 2.7–1.5 Myr and later then 1.5 Myr (<1.5 Myr). PO, Pacific Ocean; IO, Indian Ocean; AUS, Australia; AC: Agulhas Leakage.

conditions associated with a strengthening Pacific Walker Cell as well as a positive IOD mode associated with a weakening of the Indian Walker Cell (Figs. 1 and 5, 6). This would suggest the emergence of La Niña-like conditions in phase with a positive IOD across the Plio-Pleistocene transition. This finding is in line with previous suggestions of a distinct transition from permanent (e.g. Fedorov et al., 2006; Haywood et al., 2007; Wara et al., 2005) and/or variable (e.g. Watanabe et al., 2011; Zhang et al., 2014) El Niño-like conditions (with a relaxed east-west Pacific SST gradient) during the late Pliocene towards the more modern "La Niña-like" climate

(pronounced east-west SST gradient) with intensified eastern equatorial Pacific upwelling (Brierley et al., 2009; Brierley and Fedorov, 2010). In addition, an increased upwelling and cooling in the southwestern equatorial Indian Ocean has also been invoked within the Benguela region (Karas et al., 2009), which is also in line with our findings. If we apply the modern weather patterns of La Niña and positive IOD further, we may also be able to explain the quasi-synchronous SST changes between high-latitude sites ODP 882 and 1088 with the aforementioned low-latitude sites at the Plio-Pleistocene transition (Figs. 1, 5 and 6). During modern La Niña conditions, the warm water that has accumulated in the western equatorial Pacific region is traversed more rigorously into the northwest Pacific via an intensified western boundary current (Hu et al., 2015). This is fostered by the weakening of the western tropical gyre due to an SST increase, while the subpolar gyre in the western Pacific Ocean is strengthened, pumping more heat from the tropics into the high latitudes. Considering the explicit warming at site ODP 882 during the Plio-Pleistocene transition, a version of this process might also have been active in phase with the stabilizing SSTs in the western equatorial Pacific warm pool region (Fig. 6). Furthermore, a developing La Niña also fosters the development of a heat channel into the Indian Ocean though the IS via the ITF, which transports warmer and saltier water along pycnoclines directly into the western equatorial Indian Ocean (e.g., at site ODP 709), while circumventing regions in the eastern and eastern equatorial Indian Ocean (e.g., offshore western Australia; Sites ODP 758, U1460 and U1463) as well as the Arabian Sea (Fig. 6; Site ODP 722; Makarim et al., 2019). Consequently, the relative cooler SSTs over the maritime continent, opposing the warming in the western equatorial Indian Ocean, lead to the development of anomalous easterlies, which give rise to the positive IOD conditions (Behera et al., 2008). This heat channel feeds also directly into the Agulhas current and thus might explain the quasi-synchronous surface warming at site ODP 1088 in the South Atlantic to site ODP 709 in the western Indian Ocean (Fig. 4; Makarim et al., 2019). The former site is located within the vicinity of the modern Agulhas eddy pathway (Figs. 5 and 6; Caley et al., 2012). In fact, recent findings detailing the throughflow of the Mozambique Channel during the Plio-Pleistocene, a measure for the Agulhas leakage, shows a first minor strengthening at ~2.7 Ma, which persisted until ~2.4 Ma, potentially related to changes in the ocean circulation of the western equatorial Indian Ocean (van der Lubbe et al., 2021). In contrast, findings from the Benguela upwelling region suggest a strengthening of the Agulhas leakage already at ~3.2–3.0 Myr which is, however, still within the error margin of our first median change point at ~2.7 Ma (Petrick et al., 2018).

As a key role in facilitating modern SST changes in both oceans is presented by the ITF, it seems feasible to assume also that changes in the palaeo-ITF might have substantially contributed to the observed SST pattern during the Plio-to-Pleistocene transition (Smith et al., 2020). In fact, tectonically driven modifications in the geometry of the IS have been proposed for the time interval from ~5 to 3 Myr, which resulted in flow-path changes of the ITF (Fig. 6; Karas et al., 2009). In the Pacific, the IS changes are argued to have facilitated the transport of cold Subantarctic subsurface-to-intermediate waters towards the tropical East Pacific, initiating the shoaling of the thermocline and upwelling of cold water (Karas et al., 2009). This, in turn, fosters subsidence over the eastern equatorial Pacific Ocean, strengthens the easterlies that drive the accumulation of warmer water in the west and initiates La Niña-like conditions across the Pacific. On the Indian Ocean side, previous numeric model simulations suggested a cooling in the eastern equatorial Indian Ocean through the constriction of the IS (Cane and Molnar, 2001; Karas et al., 2009; Molnar and Cane, 2002), which is in line with the modern observations on the ITF heat channel (Makarim et al., 2019). The cooling of the subsurface eastern Indian Ocean was also in phase with the surface cooling of the Leeuwin Current, which receives direct inflow from the ITF (Smith et al., 2020). Recently it has been suggested that the initial ITF reorganization driven by tectonics increased the sensitivity of the ITF additionally to glacio-eustatic variability across the late Pliocene towards the early Pleistocene (Auer et al., 2019; De Vleeschouwer et al., 2018; Petrick et al., 2019). Thus, the sea level driven ITF restriction, not simply the tectonic evolution of the IS (Auer et al., 2019), lead to the irreversible cooling of the eastern Indian Ocean (Karas et al., 2009) during the late Pliocene. In fact, the long-term increase of the glacial amplitudes across the Pleistocene might have additionally contributed to restrictions in the geometry of the ITF via progressive subaerial exposure of the extensive Suhal and Sunda shelf regions (Auer et al., 2019; De Vleeschouwer et al., 2018; Di Nezio et al., 2016; Petrick et al., 2019; van der Lubbe et al., 2021).

The above outlined SST pattern dominating the Pacific and Indian Ocean continued until roughly the dominant ~2.1 Ma change point, when the majority of the studied proxy records across low and high latitudes signal a distinct change in their long-term SST variability (Figs. 4 and 5). In fact, we find that the progressive cooling trends in the eastern Pacific Ocean, the Atlantic Ocean, and the South China Sea halted and previous SST cooling trends started to stabilize, signalling the establishment of a steady-state mode of SST gradients across all major ocean basins. This would suggest that the meridional SST gradient across the Pacific and Indian Ocean reached a distinct stabilization phase characterized by a strong Pacific meridional SST gradient and weak Indian Ocean meridional SST gradient (Fig. 6). We argue that this likely indicates another phase of the WC evolution towards modern conditions that began with the Plio-Pleistocene transition. The shift in tropical SSTs at ~2.1 Ma, in contrast to the change at ~2.7 Ma, is likely not attributable to changes in the IS geometry. For instance, a dominant phase of IS restriction has been argued for the interval from 1.7 to 1.5 Myr and thus lags the SST signal evolution by roughly ~0.5 Ma (Smith et al., 2020). Furthermore, the SST evolution at ~2.1 Ma is not regionally restricted to the western tropical Pacific and Indian Ocean (as is the preceding ~2.7 Ma change point), but instead shows a more profound globally uniform character. This potentially indicates the onset of a WC mode that spans the oceanic basins of the Pacific, Indian and Atlantic Oceans synchronously.

Beyond the scope of IS modifications through tectonic or global ice volume changes, WC variability is also thought to respond to insolation as inferred from proxy records (e.g. Bush, 2007; Dang et al., 2020; Koutavas and Joanides, 2012; Zhang et al., 2007) as well as from numerical climate simulations (e.g. Clement et al., 1999; Rustic et al., 2020). The results suggest that high eccentricity/low eccentricity (increased/decreased summer insolation) align with El Niño-like/La Niña-like conditions during the Mid to Late Pleistocene (Zhang et al., 2007), respectively. Although eccentricity has only a small net effect on the annual mean insolation (less than 0.5%), it exerts a strong pull on the amplitude change of orbital precession (Laepple and Lohmann, 2009). The difference in precession amplitude can amount to ~10% of the annual mean insolation (Laskar et al., 2004). The dominant change points in orbital eccentricity during the studied time interval align with the values of 2.9 and 2.3 Myr and are within the error margins of the estimated change-point times from the analysed SST proxy records. Hence, it is possible that orbital changes contributed to both transitional shifts in WC, since during the interval from 2.9 to 2.3 Myr, a 2.4 Ma-eccentricity minimum prevailed, which coincided with exceptionally muted precession amplitudes that would favour the development of La Niña-like conditions (Zhang et al., 2007).

Independent of the ultimate cause of the WC change during the

early Pleistocene, it is worth pointing out that the co-occurrence of a strengthening WC across the Pacific and a weakening WC across the Indian Ocean – resembling simultaneous modern La Niña and positive IOD conditions – is unusual under modern climate conditions. Within the historical record (from 1900 to 2021) the co-occurrence of La Niña in combination with a positive IOD has only been observed in four seasons (1913–1914, 1967, 2007 and 2016), since usually La Niña (El Niño) favours the development of negative (positive) IOD conditions (Behera et al., 2008). Hence, the emergence and persistence of La Niña-positive IOD-like conditions during the Plio-Pleistocene transition and into the early Pleistocene hints at the fact that the sensitivity (interconnection) between the Pacific and Indian Ocean, that characterizes the modern WC, was not yet fully established during the entire investigated time period. This would suggest that during the time frame encompassing the Plio-Pleistocene transition and the early Pleistocene (i.e., our investigated time frame) only a pre-modern WC existed with variable sensitivities between the oceanic basins of the Pacific, Indian and Atlantic Oceans. As our results do not show the establishment of a WC with modern-like characteristics, in particular between the Pacific and Indian Oceans, it seems feasible to argue that the onset of a truly modern-WC only occurred later, that means, after ~1.5 Ma.

5.3. Terrestrial evidence of the proposed evolution of the Walker Circulation during the late Pliocene to mid-Pleistocene

Support for our proposed evolution of the WC from the late Pliocene towards the mid-Pleistocene (Fig. 6), as well as for a potential later-than-previously-thought onset date for the "modern" WC (i.e., post ~1.5 Ma), might be provided by terrestrial climate archives from Africa, Australia and South America. These continental regions are among the most sensitive for changes in WC based on modern climate conditions (see Section 2).

During the Plio-Pleistocene transition, western Australia was characterized by a shift to an increasingly drier climate mode, ultimately ending the humid late Pliocene conditions (Smith et al., 2020). This would be in line with cooling of the subsurface eastern Indian Ocean and the surface Leeuwin Current (Smith et al., 2020) as a consequence of increasing La Niña and positive IOD conditions (Fig. 6). On the other hand, an increase in the occurrence of deep lakes in eastern Africa, indicating wet climate conditions in this region, prevailed throughout the Plio-Pleistocene transition until roughly ~2.1–1.9 Ma, when their widespread disappearance signals the onset of drier climate conditions (Berner et al., 2022; Grant et al., 2017; Maslin et al., 2014; Trauth et al., 2005, 2009). The increase in moisture availability in eastern Africa until roughly ~2 Ma argues for the prevalence of warm SST conditions in the western Indian Ocean (e.g., Nicholson, 2017) feeding the eastern African moisture budget, similar to a modern positive IOD. Hence, the increasing east-west orientated moisture gradient across the Indian Ocean supports our assessment of a progressive Indian Ocean WC weakening until the late phase of the early Pleistocene (Fig. 6). In contrast, across the Pacific Ocean, we find that the reduction of humidity across the Andes ties closely to the development of the eastern Pacific cold tongue during the Early Pleistocene (Torres et al., 2013), and thus indicates a strengthened, La Niña-like situation of the Pacific Ocean WC (Fig. 6).

Interestingly, the onset of dryer climate conditions in East Africa starting from roughly ~2 Ma and enhancing after ~1.5 Ma (Lepre and Quinn, 2022) indicates a potential shift from positive IOD to negative IOD conditions (Fig. 6). In this scenario, a potential cooling of SSTs in the western Indian Ocean, signalling negative IOD conditions, would generate a reduced moisture content available to be transported into the neighbouring East African continent (Lepre and Quinn, 2022; Trauth et al., 2009; Maslin et al., 2014). This would also be in line with the proposed strengthening of the Indian Ocean WC after ~2.1 Ma via the Mozambique Channel throughflow (van der Lubbe et al., 2021, Fig. 6). At the same time, La Niña-like conditions most likely continued to prevail across the Pacific Ocean. The simultaneous emergence of these conditions alongside negative-IOD-like conditions across the Indian Ocean highlights the cessation of modern-type sensitivities between the Pacific and Indian Oceans between ~2.1 Ma and ~1.5 Ma. In western Australia, a shift back to wetter climate conditions has been argued after ~1 Ma, which is in line with the reinvigorating warming of the Leeuwen Current (Beck et al., 2018). Thus, a modern-type WC had most likely established in full for the first time just prior to the onset of the Mid-Pleistocene transition at ~1.25 Ma, which is also in line with previous suggestions (McClymont and Rosell-Melé, 2005). Additional support for this finding also comes from the development of the Mozambique Channel throughflow, which fully settled into its mid-Pleistocene to late-Pleistocene mode after ~1 Ma (van der Lubbe et al., 2021). This aligns with previous suggestions that negative IOD conditions strengthened the Mozambique Chanell throughflow (Ridderinkhof et al., 2010, Fig. 6). A potential driver for this mid-Pleistocene development of the WC, particular in the Indian Ocean, could be the reinvigorated tectonic activity influencing the IS geometry between 1.7 and 1.5 Myr (Smith et al., 2020). However, more research on the tectonic or global ice volume IS geometry changes during the mid-Pleistocene is needed to fully assess its potential influence on the SST variability of the Indian Ocean at that time.

6. Conclusions

Our results detail the evolution of the WC during the time interval from 3.5 to 1.5 Myr. We find that the WC experienced a multifaceted evolution with significant transitional steps at ~2.7 and ~2.1 Ma. However, these change points are not uniformly distributed across the low and high latitudes, but highlight distinct spatiotemporal patterns. A potential trigger for the development of these spatiotemporal patterns, in particular within the Indo-Pacific realm, at around ~2.7 Ma, and to a lesser extent at ~2.1 Ma, was the constriction of the IS, as this substantially changed the geometry and flow path of the ITF, which is a crucial transmitter between the Pacific and Indian Ocean. At around 2.1 Ma, the transition may have led to a combination of additional (albeit not yet clearly documented) IS restriction due to lowered global sea level and/or long-term insolation variability, in line with previous suggestions.

On a global scale, our analysis suggests that changes in low and high latitudes did, although regionally clustered, occur quasi-synchronously at ~2.7 and also at ~2.1 Ma. This suggestion supports previous assumptions that the intensification of atmospheric circulation in the tropics and subtropics contributed to the initiation of continental ice sheet formation at high latitudes. Additionally, the SST changes quantified by us had also profound effects on the adjacent continents, Africa, Australia and South America, during the studied time interval by redistributing moisture in an east-west trending pattern. Hence, our results also present a new climate framework to test current patterns of vegetation, mammal and hominin evolution events against.

Author contributions

S.K.-B. designed the study. M.M. conducted the statistical change-point regression model analysis. Both authors contributed to the discussion, figure making and the writing of the manuscript.

Data availability

All utilized data sets are available through their respective references and stored in online databases. Compressed archives of data and employed software are also available at https://www.manfredmudelsee.com.

Declaration of competing interest

The authors declare that they have no known competing financial interests or personal relationships that could have appeared to influence the work reported in this paper.

Acknowledgements

SKB acknowledges funding from the Open-Topic Post-Doc fellowship of the University of Potsdam and the Deutsche Forschungsgemeinschaft (DFG) grant number KA 4757/3–1. MM acknowledges the collegiality of Antoni Rosell i Melé, who passed away in December 2021.

References

Auer, G., De Vleeschouwer, D., Smith, R.A., Bogus, K., Groeneveld, J., Grunert, P., Castañeda, I.S., Petrick, B., Christensen, B., Fulthorpe, C., Gallagher, S.J., Henderiks, J., 2019. Timing and pacing of Indonesian throughflow restriction and its connection to late Pliocene climate shifts. Paleoceanogr. Paleoclimatol. 34, 635–657. https://doi.org/10.1029/2018PA003512.

Bahr, A., Kaboth-Bahr, S., Karas, C., 2021. The opening and closure of oceanic seaways during the Cenozoic: pacemaker of global climate change? Geological Society, London, Special Publications 523, 54. https://doi.org/10.1144/SP523-2021-54.

Bali, H., Gupta, A.K., Mohan, K., Thirumalai, K., Tiwari, S.K., Panigrahi, M.K., 2020. Evolution of the oligotrophic west Pacific warm pool during the pliocene-pleistocene boundary. Paleoceanogr. Paleoclimatol. 35, e2020PA003875. https://doi.org/10.1029/2020PA003875.

Beck, J.W., Zhou, W., Li, C., Wu, Z., White, L., Xian, F., Kong, X., An, Z., 2018. A 550,000-year record of East Asian monsoon rainfall from ^{10}Be in loess. Science 360, 877–881. https://doi.org/10.1126/science.aam5825.

Behera, S.K., Luo, J.-J., Yamagata, T., 2008. Unusual IOD event of 2007. Geophys. Res. Lett. 35, L14S11. https://doi.org/10.1029/2008GL034122.

Bell, D.B., Jung, S.J.A., Kroon, D., 2015. The Plio-Pleistocene development of Atlantic deep-water circulation and its influence on climate trends. Quat. Sci. Rev. 123, 265–282. https://doi.org/10.1016/j.quascirev.2015.06.026.

Berner, N., Trauth, M.H., Holschneider, M., 2022. Bayesian inference about Plio-Pleistocene climate transitions in Africa. Quat. Sci. Rev. 277, 107287. https://doi.org/10.1016/j.quascirev.2021.107287.

Bjerknes, J., 1966. A possible response of the atmospheric Hadley circulation to equatorial anomalies of ocean temperature. Tellus 18, 820–829. https://doi.org/10.3402/tellusa.v18i4.9712.

Bjerknes, J., 1969. Atmospheric teleconnections from the equatorial Pacific. Mon. Weather Rev. 97, 163–172. https://doi.org/10.1175/1520-0493(1969)097<0163:atftep>2.3.co, 2.

Bodart, J.A., Bingham, R.J., 2019. The impact of the extreme 2015–2016 El Niño on the mass balance of the Antarctic ice sheet. Geophys. Res. Lett. 46, 13862–13871. https://doi.org/10.1029/2019GL084466.

Brierley, C.M., Fedorov, A.V., 2010. Relative importance of meridional and zonal sea surface temperature gradients for the onset of the ice ages and Pliocene-Pleistocene climate evolution. Paleoceanography 25, PA2214. https://doi.org/10.1029/2009PA001809.

Brierley, C.M., Fedorov, A.V., Liu, Z., Herbert, T.D., Lawrence, K.T., LaRiviere, J.P., 2009. Greatly expanded tropical warm pool and weakened Hadley Circulation in the Early Pliocene. Science 323, 1714–1718. https://doi.org/10.1126/science.1167625.

Bush, A.B.G., 2007. Extratropical influences on the El Niño–Southern oscillation through the late quaternary. J. Clim. 20, 788–800. https://doi.org/10.1175/JCLI4048.1.

Caley, T., Giraudeau, J., Malaizé, B., Rossignol, L., Pierre, C., 2012. Agulhas leakage as a key process in the modes of Quaternary climate changes. Proc. Natl. Acad. Sci. U. S. A. 109, 6835–6839. https://doi.org/10.1073/pnas.1115545109.

Cane, M.A., 1998. A role for the tropical Pacific. Science 282, 59–61. https://doi.org/10.1126/science.282.5386.59.

Cane, M.A., Molnar, P., 2001. Closing of the Indonesian seaway as a precursor to east African aridification around 3–4 million years ago. Nature 411, 157–162. https://doi.org/10.1038/35075500.

Cannariato, K.G., Ravelo, A.C., 1997. Pliocene-Pleistocene evolution of eastern tropical Pacific surface water circulation and thermocline depth. Paleoceanography 12, 805–820. https://doi.org/10.1029/97PA02514.

Chang, P., Fang, Y., Saravanan, R., Ji, L., Seidel, H., 2006. The cause of the fragile relationship between the pacific El Niño and the Atlantic Niño. Nature 443, 324–328. https://doi.org/10.1038/nature05053.

Cheng, X., Zhao, Q., Wang, J., Jian, Z., Xia, P., Huang, B., Fang, D., Xu, J., Zhou, Z., Wang, P., 2004. Data report: stable isotopes from sites 1147 and 1148. Proc. Ocean Drill. Progr. Sci. Results 184, 1–12. https://doi.org/10.2973/odp.proc.sr.184.223.2004.

Church, M.J., Wai, B., Karl, D.M., DeLong, E.F., 2010. Abundances of crenarchaeal amoA genes and transcripts in the Pacific Ocean. Environ. Microbiol. 12, 679–688. https://doi.org/10.1111/j.1462-2920.2009.02108.x.

Clement, A.C., Seager, R., Cane, M.A., 1999. Orbital controls on the El Niño/Southern oscillation and the tropical climate. Paleoceanography 14, 441–456. https://doi.org/10.1029/1999PA900013.

Dang, H., Jian, Z., Wang, Y., Mohtadi, M., Rosenthal, Y., Ye, L., Bassinot, F., Kuhnt, W., 2020. Pacific warm pool subsurface heat sequestration modulated Walker circulation and ENSO activity during the Holocene. Sci. Adv. 6, eabc0402. https://doi.org/10.1126/sciadv.abc0402.

deMenocal, P.B., 2012. The Ocean's Role in the Early Pleistocene Aridification of East Africa American Association for the Advancement of Science Annual Meeting. Vancouver, Canada. https://aaas.confex.com/aaas/2012/webprogram/Paper6488.html.

De Vleeschouwer, D., Auer, G., Smith, R., Bogus, K., Christensen, B., Groeneveld, J., Petrick, B., Henderiks, J., Castañeda, I.S., O'Brien, E., Ellinghausen, M., Gallagher, S.J., Fulthorpe, C.S., Pälike, H., 2018. The amplifying effect of Indonesian Throughflow heat transport on Late Pliocene Southern Hemisphere climate cooling. Earth Planet Sci. Lett. 500, 15–27. https://doi.org/10.1016/j.epsl.2018.07.035.

de Oliveira, C.P., Aímola, L., Ambrizzi, T., Freitas, A.C.V., 2018. The influence of the regional Hadley and Walker circulations on precipitation patterns over Africa in El Niño, La Niña, and neutral years. Pure Appl. Geophys. 175, 2293–2306. https://doi.org/10.1007/s00024-018-1782-4.

Di Nezio, P.N., Timmermann, A., Tierney, J.E., Jin, F.F., Otto-Bliesner, B., Rosenbloom, N., Mapes, B., Neale, R., Ivanovic, R.F., Montenegro, A., 2016. The climate response of the Indo-Pacific warm pool to glacial sea level. Paleoceanography 31, 866–894. https://doi.org/10.1002/2015PA002890.

Etourneau, J., Martinez, P., Blanz, T., Schneider, R., 2009. Pliocene-Pleistocene variability of upwelling activity, productivity, and nutrient cycling in the Benguela region. Geology 37, 871–874. https://doi.org/10.1130/G25733A.1.

Etourneau, J., Schneider, R., Blanz, T., Martinez, P., 2010. Intensification of the Walker and Hadley atmospheric circulations during the Pliocene–Pleistocene climate transition. Earth Planet Sci. Lett. 297, 103–110. https://doi.org/10.1016/j.epsl.2010.06.010.

Farmer, E.C., deMenocal, P.B., Marchitto, T.M., 2005. Holocene and deglacial ocean temperature variability in the Benguela upwelling region: implications for low-latitude atmospheric circulation. Paleoceanography 20, PA2018. https://doi.org/10.1029/2004PA001049.

Farrell, J.W., Janecek, T.R., 1991. Late Neogene paleoceanography and paleoclimatology of the northeast Indian ocean (site 758). Proc. Ocean Drill. Progr. Sci. Results 121, 297–355. https://doi.org/10.2973/odp.proc.sr.121.124.1991.

Fedorov, A.V., Dekens, P.S., McCarthy, M., Ravelo, A.C., deMenocal, P.B., Barreiro, M., Pacanowski, R.C., Philander, S.G., 2006. The Pliocene paradox (mechanisms for a permanent El Niño). Science 312, 1485–1489. https://doi.org/10.1126/science.1122666.

Ford, H.L., Ravelo, A.C., Dekens, P.S., Lariviere, J.P., Wara, M.W., 2015. The evolution of the equatorial thermocline and the early Pliocene El Padre mean state. Geophys. Res. Lett. 42, 4878–4887. https://doi.org/10.1002/2015GL064215.

Grant, K.M., Rohling, E.J., Westerhold, T., Zabel, M., Heslop, D., Konijnendijk, T., Lourens, L., 2017. A 3 million year index for North African humidity/aridity and the implication of potential pan-African humid periods. Quat. Sci. Rev. 171, 100–118. https://doi.org/10.1016/j.quascirev.2017.07.005.

Haug, G.H., 1996. Dissertation: Zur Palāo-Ozeanographie und Sedimentationsgeschichte im Nordwest-Pazifik während der letzten 6 Millionen Jahre (ODP-Site 882). PhD Dissertation, Christian-Albrechts-Universität zu Kiel, Germany.

Haug, G.H., Tiedemann, R., 1998. Effect of the formation of the isthmus of Panama on Atlantic Ocean thermohaline circulation. Nature 393, 673–676. https://doi.org/10.1038/31447.

Haug, G.H., Sigman, D.M., Tiedemann, R., Pedersen, T.F., Sarnthein, M., 1999. Onset of permanent stratification in the subarctic Pacific Ocean. Nature 401, 779–782. https://doi.org/10.1038/44550.

Haug, G.H., Tiedemann, R., Zahn, R., Ravelo, A.C., 2001. Role of Panama uplift on oceanic freshwater balance. Geology 29, 207–210. https://doi.org/10.1130/0091-7613(2001)029<0207:ROPUOO>2.0.CO, 2.

Haywood, A.M., Valdes, P.J., Peck, V.L., 2007. A permanent El Niño-like state during the Pliocene? Paleoceanography 22, PA1213. https://doi.org/10.1029/2006PA001323.

Herbert, T.D., Schuffert, J.D., Thomas, D., Lange, C., Weinheimer, A., Peleo-Alampay, A., Herguera, J.-C., 1998. Depth and seasonality of alkenone production along the California margin inferred from a core top transect. Paleoceanography 13, 263–271. https://doi.org/10.1029/98PA00069.

Herbert, T.D., Peterson, L.C., Lawrence, K.T., Liu, Z., 2010. Tropical ocean temperatures over the past 3.5 million years. Science 328, 1530–1534. https://doi.org/10.1126/science.1185435.

Herbert, T.D., Lawrence, K.T., Tzanova, A., Peterson, L.C., Caballero-Gill, R., Kelly, C.S., 2016. Late Miocene global cooling and the rise of modern ecosystems. Nat. Geosci. 9, 843–847. https://doi.org/10.1038/ngeo2813.

Hertzberg, J.E., Schmidt, M.W., Bianchi, T.S., Smith, R.K., Shields, M.R., Marcantonio, F., 2016. Comparison of eastern tropical Pacific TEX86 and Globigerinoides ruber Mg/Ca derived sea surface temperatures: insights from the Holocene and Last Glacial Maximum. Earth Planet Sci. Lett. 434, 320–332. https://doi.org/10.1016/j.epsl.2015.11.050.

Hu, D., Wu, L., Cai, W., Gupta, A.S., Ganachaud, A., Qiu, B., Gordon, A.L., Lin, X., Chen, Z., Hu, S., Wang, G., Wang, Q., Sprintall, J., Qu, T., Kashino, Y., Wang, F., Kessler, W.S., 2015. Pacific western boundary currents and their roles in climate. Nature 522, 299–308. https://doi.org/10.1038/nature14504.

Inglis, G.N., Tierney, J.E., 2020. The TEX86 Paleotemperature Proxy. Cambridge Univ. Press, Cambridge, p. 25. https://doi.org/10.1017/9781108846998.

Jansen, E., Mayer, L.A., Backman, J., Leckie, R.M., Takayama, T., 1993. Evolution of Pliocene climate cyclicity at hole 806B (5–2 Ma): oxygen isotope record. Proc. Ocean Drill. Progr. Sci. Results 349–362. https://doi.org/10.2973/odp.proc.sr.130.028.1993.

Joyce, J.E., Tjalsma, L.R.C., Prutzman, J.M., 1990. High-resolution planktic stable isotope record and spectral analysis for the last 5.35 M.Y.: Ocean Drilling Program Site 625 northeast Gulf of Mexico. Paleoceanography 5, 507–529. https://doi.org/10.1029/PA005i004p00507.

Kaboth-Bahr, S., Gosling, W.D., Vogelsang, R., Bahr, A., Scerri, E.M.L., Asrat, A., Cohen, A.S., Düsing, W., Foerster, V., Lamb, H.F., Maslin, M.A., Roberts, H.M., Schäbitz, F., Trauth, M.H., 2021. Paleo-ENSO influence on African environments and early modern humans. Proc. Natl. Acad. Sci. U. S. A. 118, e2018277118. https://doi.org/10.1073/pnas.2018277118.

Karas, C., Nürnberg, D., Gupta, A.K., Tiedemann, R., Mohan, K., Bickert, T., 2009. Mid-Pliocene climate change amplified by a switch in Indonesian subsurface throughflow. Nat. Geosci. 2, 434–438. https://doi.org/10.1038/ngeo520.

Keigwin, L., 1982. Isotopic paleoceanography of the Caribbean and East Pacific: role of Panama uplift in Late Neogene time. Science 217, 350–353. https://doi.org/10.1126/science.217.4557.350.

Koutavas, A., Joanides, S., 2012. El Niño–Southern Oscillation extrema in the Holocene and Last Glacial Maximum. Paleoceanography 27, PA4208. https://doi.org/10.1029/2012PA002378.

Künsch, H.R., 1989. The jackknife and the bootstrap for general stationary observations. Ann. Stat. 17, 1217–1241. https://doi.org/10.1214/aos/1176347265.

Laepple, T., Lohmann, G., 2009. Seasonal cycle as template for climate variability on astronomical timescales. Paleoceanography 24, PA4201. https://doi.org/10.1029/2008PA001674.

Laskar, J., Robutel, P., Joutel, F., Gastineau, M., Correia, A.C.M., Levrard, B., 2004. A long-term numerical solution for the insolation quantities of the Earth. Astron. Astrophys. 428, 261–285. https://doi.org/10.1051/0004-6361:20041335.

Lau, K.-M., Yang, S., 2003. Walker circulation. In: Encyclopedia of Atmospheric Sciences. Elsevier, pp. 2505–2510. https://doi.org/10.1016/B0-12-227090-8/00450-4.

Lawrence, K.T., Liu, Z., Herbert, T.D., 2006. Evolution of the eastern tropical Pacific through Plio-Pleistocene glaciation. Science 312, 79–83. https://doi.org/10.1126/science.1120395.

Lawrence, K.T., Herbert, T.D., Brown, C.M., Raymo, M.E., Haywood, A.M., 2009. High-amplitude variations in North Atlantic sea surface temperature during the early Pliocene warm period. Paleoceanography 24, PA2218. https://doi.org/10.1029/2008PA001669.

Lea, D.W., 2014. Elemental and isotopic proxies of past ocean temperatures. In: Holland, H.D., Turekian, K.K. (Eds.), Treatise on Geochemistry, second ed., 8. Elsevier, Amsterdam, pp. 373–397. https://doi.org/10.1016/B978-0-08-095975-7.00614-8.

Lepre, C.J., Quinn, R.L., 2022. Aridification and orbital forcing of eastern African climate during the Plio-Pleistocene. Global Planet. Change 208. https://doi.org/10.1016/j.gloplacha.2021.103684.

Li, L., Li, Q., Tian, J., Wang, P., Wang, H., Liu, Z., 2011. A 4-Ma record of thermal evolution in the tropical western Pacific and its implications on climate change. Earth Planet Sci. Lett. 309, 10–20. https://doi.org/10.1016/j.epsl.2011.04.016.

Lisiecki, L.E., Raymo, M.E., 2005. A Pliocene-Pleistocene stack of 57 globally distributed benthic $\delta^{18}O$ records. Paleoceanography 20, PA1003. https://doi.org/10.1029/2004PA001071.

Liu, J., Curry, J.A., Hu, Y., 2004. Recent Arctic sea ice variability: connections to the Arctic oscillation and the ENSO. Geophys. Res. Lett. 31, L09211. https://doi.org/10.1029/2004GL019858.

Liu, J., Tian, J., Liu, Z., Herbert, T.D., Fedorov, A.V., Lyle, M., 2019. Eastern equatorial Pacific cold tongue evolution since the late Miocene linked to extratropical climate. Sci. Adv. 5, eaau6060. https://doi.org/10.1126/sciadv.aau6060.

Luo, J.-J., Masson, S., Behera, S.K., Yamagata, T., 2008. Extended ENSO predictions using a fully coupled ocean–atmosphere model. J. Clim. 21, 84–93. https://doi.org/10.1175/2007JCLI1412.1.

Lüthi, D., Le Floch, M., Bereiter, B., Blunier, T., Barnola, J.-M., Siegenthaler, U., Raynaud, D., Jouzel, J., Fischer, H., Kawamura, K., Stocker, T.F., 2008. High-resolution carbon dioxide concentration record 650,000–800,000 years before present. Nature 453, 379–382. https://doi.org/10.1038/nature06949.

Makarim, S., Sprintall, J., Liu, Z., Yu, W., Santoso, A., Yan, X.-H., Susanto, R.D., 2019. Previously unidentified Indonesian Throughflow pathways and freshening in the Indian Ocean during recent decades. Sci. Rep. 9, 7364. https://doi.org/10.1038/s41598-019-43841-z.

Martínez-Garcia, A., Rosell-Melé, A., McClymont, E.L., Gersonde, R., Haug, G.H., 2010. Subpolar link to the emergence of the modern equatorial Pacific cold tongue. Science 328, 1550–1553. https://doi.org/10.1126/science.1184480.

Maslin, M.A., Brierley, C.M., Milner, A.M., Shultz, S., Trauth, M.H., Wilson, K.E., 2014. East African climate pulses and early human evolution. Quat. Sci. Rev. 101, 1–17. https://doi.org/10.1016/j.quascirev.2014.06.012.

McClymont, E.L., Rosell-Melé, A., 2005. Links between the onset of modern Walker circulation and the mid-Pleistocene climate transition. Geology 33, 389–392. https://doi.org/10.1130/G21292.1.

Molnar, P., Cane, M.A., 2002. El Niño's tropical climate and teleconnections as a blueprint for pre-ice age climates. Paleoceanography 17, PA1021. https://doi.org/10.1029/2001pa000663.

Mudelsee, M., 2000. Ramp function regression: a tool for quantifying climate transitions. Comput. Geosci. 26, 293–307. https://doi.org/10.1016/S0098-3004(99)00141-7.

Mudelsee, M., 2002. TAUEST: a computer program for estimating persistence in unevenly spaced weather/climate time series. Comput. Geosci. 28, 69–72. https://doi.org/10.1016/S0098-3004(01)00041-3.

Mudelsee, M., 2014. Climate Time Series Analysis: Classical Statistical and Bootstrap Methods, second ed. Springer, Cham, Switzerland, p. 454. https://doi.org/10.1007/978-3-319-04450-7.

Mudelsee, M., Raymo, M.E., 2005. Slow dynamics of the Northern Hemisphere glaciation. Paleoceanography 20, PA4022. https://doi.org/10.1029/2005PA001153.

Murray, D.W., Prell, W.L., 1991. Pliocene to Pleistocene variations in calcium carbonate, organic carbon, and opal on the Owen Ridge, northern Arabian Sea. Proc. Ocean Drill. Progr. Sci. Results 117, 343–363. https://doi.org/10.2973/odp.proc.sr.117.141.1991.

Newton, I., 1687. Philosophiae Naturalis Principia Mathematica. Jussu Societatis Regiae ac Typis Josephi Streater, London, p. 510.

Nicholson, S.E., 2017. Climate and climatic variability of rainfall over eastern Africa. Rev. Geophys. 55, 590–635. https://doi.org/10.1002/2016RG000544.

Nürnberg, D., Bijma, J., Hemleben, C., 1996. Assessing the reliability of magnesium in foraminiferal calcite as a proxy for water mass temperatures. Geochem. Cosmochim. Acta 60, 803–814. https://doi.org/10.1016/0016-7037(95)00446-7.

O'Brien, C.L., Foster, G.L., Martínez-Botí, M.A., Abell, R., Rae, J.W.B., Pancost, R.D., 2014. High sea surface temperatures in tropical warm pools during the Pliocene. Nat. Geosci. 7, 606–611. https://doi.org/10.1038/ngeo2194.

Pausata, F.S.R., Zhang, Q., Muschitiello, F., Lu, Z., Chafik, L., Niedermeyer, E.M., Stager, J.C., Cobb, K.M., Liu, Z., 2017. Greening of the Sahara suppressed ENSO activity during the mid-Holocene. Nat. Commun. 8, 16020. https://doi.org/10.1038/ncomms16020.

Petrick, B., McClymont, E.L., Littler, K., Rosell-Melé, A., Clarkson, M.O., Maslin, M., Röhl, U., Shevenell, A.E., Pancost, R.D., 2018. Oceanographic and climatic evolution of the southeastern subtropical Atlantic over the last 3.5 Ma. Earth Planet Sci. Lett. 492, 12–21. https://doi.org/10.1016/j.epsl.2018.03.054.

Petrick, B., Martínez-García, A., Auer, G., Reuning, L., Auderset, A., Deik, H., Takayanagi, H., De Vleeschouwer, D., Iryu, Y., Haug, G.H., 2019. Glacial Indonesian throughflow weakening across the Mid-Pleistocene climatic transition. Sci. Rep. 9, 16995. https://doi.org/10.1038/s41598-019-53382-0.

Prahl, F.G., Muehlhausen, L.A., Zahnle, D.L., 1988. Further evaluation of long-chain alkenones as indicators of paleoceanographic conditions. Geochem. Cosmochim. Acta 52, 2303–2310. https://doi.org/10.1016/0016-7037(88)90132-9.

Ravelo, A.C., Hillaire-Marcel, C., 2007. The use of oxygen and carbon isotopes of foraminifera in paleoceanography. In: Hillaire-Marcel, C., De Vernal, A. (Eds.), Developments in Marine Geology, 1. Amsterdam Elsevier, pp. 735–763. https://doi.org/10.1016/S1572-5480(07)01023-8.

Ravelo, A.C., Andreasen, D.H., Lyle, M., Lyle, A.O., Wara, M.W., 2004. Regional cflimate shifts caused by gradual global cooling in the Pliocene epoch. Nature 429, 263–267. https://doi.org/10.1038/nature02567.

Raymo, M.E., Ruddiman, W.F., 1992. Tectonic forcing of late Cenozoic climate. Nature 359, 117–122. https://doi.org/10.1038/359117a0.

Regenberg, M., Nürnberg, D., Steph, S., Groeneveld, J., Garbe-Schönberg, D., Tiedemann, R., Dullo, W.-C., 2006. Assessing the effect of dissolution on planktonic foraminiferal Mg/Ca ratios: evidence from Caribbean core tops. G-cubed 7, Q07P15. https://doi.org/10.1029/2005GC001019.

Ridderinkhof, H., Van der Werf, P.M., Ullgren, J.E., Van Aken, H.M., Van Leeuwen, P.J., De Ruijter, W.P.M., 2010. Seasonal and interannual variability in the Mozambique Channel from moored current observations. J. Geophys. Res.: Oceans 115, C06010. https://doi.org/10.1029/2009JC005619.

Rustic, G.T., Polissar, P.J., Ravelo, A.C., White, S.M., 2020. Modulation of late Pleistocene ENSO strength by the tropical Pacific thermocline. Nat. Commun. 11, 5377. https://doi.org/10.1038/s41467-020-19161-6.

Schouten, S., Hopmans, E.C., Schefuß, E., Sinninghe Damsté, J.S., 2002. Distributional variations in marine crenarchaeotal membrane lipids: a new tool for reconstructing ancient sea water temperatures? Earth Planet Sci. Lett. 204, 265–274. https://doi.org/10.1016/S0012-821X(02)00979-2.

Shackleton, N.J., 1987. Oxygen isotopes, ice volume and sea level. Quat. Sci. Rev. 6, 183–190. https://doi.org/10.1016/0277-3791(87)90003-5.

Shackleton, N.J., Hall, M.A., 1990. Pliocene oxygen isotope stratigraphy of Hole 709C. Proc. Ocean Drill. Progr. Sci. Results 115, 529–538. https://doi.org/10.2973/odp.proc.sr.115.174.1990.

Shackleton, N.J., Backman, J., Zimmerman, H., Kent, D.V., Hall, M.A., Roberts, D.G., Schnitker, D., Baldauf, J.G., Desprairies, A., Homrighausen, R., Huddlestun, P., Keene, J.B., Kaltenback, A.J., Krumsiek, K.A.O., Morton, A.C., Murray, J.W., Westberg-Smith, J., 1984. Oxygen isotope calibration of the onset of ice-rafting and history of glaciation in the North Atlantic region. Nature 307, 620–623. https://doi.org/10.1038/307620a0.

Singh, R.K., Gupta, A.K., Das, M., Flower, B.P., 2021. Paleoceanographic turnovers

during the Plio-Pleistocene in the southeastern Indian Ocean: linkages with Northern Hemisphere glaciation and Indian Monsoon variability. Palaeogeogr. Palaeoclimatol. Palaeoecol. 571, 110374. https://doi.org/10.1016/j.palaeo.2021.110374.

Smith, R.A., Castañeda, I.S., Groeneveld, J., De Vleeschouwer, D., Henderiks, J., Christensen, B.A., Renema, W., Auer, G., Bogus, K., Gallagher, S.J., Fulthorpe, C.S., 2020. Plio-Pleistocene Indonesian Throughflow variability drove eastern Indian Ocean sea surface temperatures. Paleoceanogr. Paleoclimatol. 35, e2020PA003872. https://doi.org/10.1029/2020PA003872.

Tierney, J.E., Haywood, A.M., Feng, R., Bhattacharya, T., Otto-Bliesner, B.L., 2019. Pliocene warmth consistent with greenhouse gas forcing. Geophys. Res. Lett. 46, 9136–9144. https://doi.org/10.1029/2019GL083802.

Torres, V., Hooghiemstra, H., Lourens, L., Tzedakis, P.C., 2013. Astronomical tuning of long pollen records reveals the dynamic history of montane biomes and lake levels in the tropical high Andes during the Quaternary. Quat. Sci. Rev. 63, 59–72. https://doi.org/10.1016/j.quascirev.2012.11.004.

Trauth, M.H., Maslin, M.A., Deino, A., Strecker, M.R., 2005. Late Cenozoic moisture history of East Africa. Science 309, 2051–2053. https://doi.org/10.1126/science.1112964.

Trauth, M.H., Maslin, M.A., Deino, A.L., Strecker, M.R., Bergner, A.G.N., Dühnforth, M., 2007. High- and low-latitude forcing of Plio-Pleistocene East African climate and human evolution. J. Hum. Evol. 53, 475–486. https://doi.org/10.1016/j.jhevol.2006.12.009.

Trauth, M.H., Larrasoaña, J.C., Mudelsee, M., 2009. Trends, rhythms and events in Plio-Pleistocene African climate. Quat. Sci. Rev. 28, 399–411. https://doi.org/10.1016/j.quascirev.2008.11.003.

Trauth, M.H., Bergner, A.G.N., Foerster, V., Junginger, A., Maslin, M.A., Schaebitz, F., 2015. Episodes of environmental stability versus instability in Late Cenozoic lake records of Eastern Africa. J. Hum. Evol. 87, 21–31. https://doi.org/10.1016/j.jhevol.2015.03.011.

Urey, H.C., 1947. The thermodynamic properties of isotopic substances. J. Chem. Soc. 562–581. https://doi.org/10.1039/JR9470000562.

van Oldenborgh, G.J., Philip, S.Y., Collins, M., 2005. El Niño in a changing climate: a multi-model study. Ocean Sci. 1, 81–95. https://doi.org/10.5194/os-1-81-2005.

van der Lubbe, H.J.L., Hall, H.J.L., Barker, S., Hemming, S.R., Baars, T.F., Starr, A., Just, J., Backeberg, B.C., Joordens, J.C.A., 2021. Indo-Pacific Walker circulation drove Pleistocene African aridification. Nature 598, 618–623. https://doi.org/10.1038/s41586-021-03896-3.

Villanueva, L., Schouten, S., Sinninghe Damsté, J.S., 2015. Depth-related distribution of a key gene of the tetraether lipid biosynthetic pathway in marine Thaumarchaeota. Environ. Microbiol. 17, 3527–3539. https://doi.org/10.1111/1462-2920.12508.

Walker, G.T., 1923. Correlation in seasonal variations of weather, VIII: a preliminary study of world-weather. Mem. Ind. Meteor. Dept. 24, 75–131.

Wara, M.W., Ravelo, A.C., Delaney, M.L., 2005. Permanent El Niño-like conditions during the Pliocene warm period. Science 309, 758–761. https://doi.org/10.1126/science.1112596.

Watanabe, T., Suzuki, A., Minobe, S., Kawashima, T., Kameo, K., Minoshima, K., Aguilar, Y.M., Wani, R., Kawahata, H., Sowa, K., Nagai, T., Kase, T., 2011. Permanent El Niño during the Pliocene warm period not supported by coral evidence. Nature 471, 209–211. https://doi.org/10.1038/nature09777.

Webster, P.J., 1983. The large scale structure of the tropical atmosphere. In: Hoskins, B., Pearce, R. (Eds.), General Circulation of the Atmosphere. Academic Press, San Diego, pp. 235–275.

Whitman, J.M., Berger, W.H., 1992. Pliocene-Pleistocene oxygen isotope record site 586, Ontong Java Plateau. Mar. Micropaleontol. 18, 171–198. https://doi.org/10.1016/0377-8398(92)90012-9.

Wuchter, C., Schouten, S., Coolen, M.J.L., Sinninghe Damsté, J.S., 2004. Temperature-dependent variation in the distribution of tetraether membrane lipids of marine Crenarchaeota: implications for TEX86 paleothermometry. Paleoceanography 19, PA4028. https://doi.org/10.1029/2004PA001041.

Zhang, Y.G., Ji, J., Balsam, W.L., Liu, L., Chen, J., 2007. High resolution hematite and goethite records from ODP 1143, South China Sea: Co-evolution of monsoonal precipitation and El Niño over the past 600,000 years. Earth Planet Sci. Lett. 264, 136–150. https://doi.org/10.1016/j.epsl.2007.09.022.

Zhang, Y.G., Pagani, M., Liu, Z., 2014. A 12-million-year temperature history of the tropical Pacific Ocean. Science 344, 84–87. https://doi.org/10.1126/science.1246172.

Zhang, W., Wang, Y., Jin, F.-F., Stuecker, M.F., Turner, A.G., 2015. Impact of different El Niño types on the El Niño/IOD relationship. Geophys. Res. Lett. 42, 8570–8576. https://doi.org/10.1002/2015GL065703.